Structural revision of the Mcl-1 inhibitor MIM1: synthesis and biological studies on ovarian cancer cells with evaluation of designed analogues

Hippolyte Paysant, Siham Hedir, Frédéric Justaud, Louis Bastien Weiswald, Assaad Nasr El Dine, Ali Soulieman, Ali Hachem, Nicolas Elie, Emilie Brotin, Christophe Denoyelle, et al.

Structural revision of the Mcl-1 inhibitor MIM1. Synthesis and biological studies on ovarian cancer cells with evaluation of designed analogues

Hippolyte Paysant[1,2■], Siham Hedir[1,2■], Frédéric Justaud[3], Louis Bastien Weiswald[1,2], Assaad Nasr El Dine[3,4], Ali Soulieman[3,4], Ali Hachem[4], Nicolas Elie[5], Emilie Brotin[1,2,5], Christophe Denoyelle[1,2,5], Jérôme Bignon[7], Fanny Roussi[7], Marie Jouanne[8], Olivier Tasseau[3], Thierry Roisnel[3], Anne Sophie Voisin-Chiret[8*], René Grée[3*], Nicolas Levoin[9*] and Laurent Poulain[1,2*]

Abstract: In the cancer research area, the development of new and potent inhibitors of anti-apoptotic proteins is a very active and promising topic. The small molecule MIM1 has been reported earlier as one of the first selective inhibitors of the anti-apoptotic protein Mcl-1. In the present paper we first revised the structure of this molecule, based on extensive physicochemical analyses. Then, we designed and synthetized a focused library of analogues for the corrected structure of MIM1. Next, these molecules were submitted to a panel of *in cellulo* biological studies, allowing the identification of dual Bcl-x_L/Mcl-1 inhibitors, as well as selective Mcl-1 inhibitors. These results have been complemented by Fluorescence Polarization Assays with Mcl-1 protein. Preliminary Structure-Activity Relationships were discussed and extensive molecular modelling studies allowed us to propose a rationale for the biological activity of this series of new inhibitors, in particular for the selectivity of inhibition of Mcl-1 *versus* Bcl-x_L.

Introduction

Despite advances in the field of anticancer strategies over the last decade, cancer malignancies remain responsible for 10 million deaths each year worldwide (WHO). Overcoming resistance of cancer cells to conventional treatment is a major challenge in oncology, and innovative strategies are required for this purpose.[1]

Since apoptotic cell death deregulations are frequently involved both in carcinogenesis and chemoresistance, the development of innovative pro-apoptotic strategies has been the subject of numerous excellent studies within the last decade. One of the most exciting fields of investigations concerns the inhibition of expression, or activity, of anti-apoptotic proteins of the Bcl-2 family, particularly Bcl-x_L, Bcl-2 and Mcl-1.

Bcl-2 family members share homology in their conserved Bcl-2 homology domains (BH1 to BH4), and belong to both anti-apoptotic and pro-apoptotic proteins. Pro-apoptotic pore-formers proteins (Bax, Bak) include BH1 to BH3 domains, while BH3-only pro-apoptotic proteins (Bim, Bid, Bad, Puma, Noxa, Hrk etc.) conserve only the BH3 domain. Anti-apoptotic proteins (Bcl-2, Bcl-x_L, Mcl-1, Bcl-w, A1 and Bfl-1) contain the BH1 to BH4 domains. In response to death signals, the BH3-only proteins

[1] *Normandie Univ, UNICAEN, Inserm U1086 ANTICIPE «Unité de Recherche Interdisciplinaire pour la Prévention et le Traitement des Cancers», Caen, France*
[2] *UNICANCER, Centre de Lutte Contre le Cancer F. Baclesse, 3 avenue du Général Harris, 14076, Caen, France.*
[3] *Univ Rennes, CNRS, ISCR (Institut des Sciences Chimiques de Rennes), UMR 6226, F-35000, Rennes, France.*
[4] *Laboratoire de Chimie Médicinale et de Produits Naturels, Université Libanaise, Faculté des Sciences et PRASE-EDST, Hadath, Beyrouth, Liban.*
[5] *Normandie Univ, UNICAEN, SF 4206 ICORE, CMABIO3, Caen, France.*
[6] *Normandie Univ, UNICAEN, SF4206 ICORE, Plateforme ImpedanCELL, Caen, France.*
[7] *Institut de Chimie des Substances Naturelles CNRS UPR 2301, Université Paris Saclay, Gif-sur-Yvette, France.*
[8] *Normandie Univ, UNICAEN, Centre d'Etudes et de Recherche sur le Médicament de Normandie (CERMN), 14000 Caen, France.*
[9] *Bioprojet-Biotech, 4 rue du Chesnay Beauregard, BP 96205, 35762, Saint Grégoire, France.*
■ *Equal contribution to this work*
**co-corresponding authors*

† Electronic Supplementary Information (ESI) available: Copies of the ^{1}H and ^{13}C NMR spectra for all molecules, plus 2D NMR spectra and extra NMR experiments to establish the structure of MIM1 (**2)** and X-Ray analysis data for **11**, **14a** and **14b**. Are included also the SI Fig. 5: Effect of ABT-737 and S63845 combination on IGROV1-R10 cell line, the SI Fig. 6 & Fig 7: determination of Bcl-x_L binding site by molecular modelling and the SI Fig 8: Computational studies of compound **35** onto Mcl-1 and Bcl-x_L. See DOI: 10.1039/x0xx00000x

are activated (expression, localisation or conformational changes) and antagonise the function of anti-apoptotic proteins through the interaction of the α-helix of their BH3 domain with the hydrophobic groove of anti-apoptotic proteins. This interaction leads to the release of the multidomain members Bax and Bak from their anti-apoptotic trapper and to their subsequent pro-apoptotic activity. Some BH3-only proteins, such as Bim or Puma, are able to directly activate Bax and Bak, thus leading to apoptosis, provided that activated Bax and Bak are not sequestered by anti-apoptotic proteins.[2]

Anti-apoptotic Bcl-2 family proteins are overexpressed in human cancers[3] and are frequently associated with resistance to conventional chemotherapies, as well as targeted therapies.[4] The oncological scientific community thus focused its attention on these possible targets in order to identify selective pharmacological inhibitors.[5, 6] For this purpose, one approach is to mimic the BH3 domain of the pro-apoptotic proteins, such molecules being thus called "BH3-mimetics". Numerous studies have shown that inhibition of the expression, or activity, of these targets can lead to apoptotic cell death in cancer cells,[7-9] as well as to sensitise them to various anti-tumor agents.[10-15]

Clinical trials have been performed within the last decade with BH3 mimetics directed against Bcl-x_L (ABT-263/Navitoclax),[16] Bcl-2 (ABT-199/Venetoclax)[17] and more recently Mcl-1 (MIK665/S64315, AMG176, AZD5991),[18] leading to the approval of Venetoclax by the Food and Drug Administration (FDA) for cancer treatment of patients with chronic lymphocytic leukemia and acute myeloid leukemia.[19] In these trials, BH3-mimetics were mainly used as single agents in hematological malignancies. However multiple preclinical studies, including ours, also showed that they could be interestingly combined together,[20-22] as well as with other antitumor agents such as conventional chemotherapeutic agents[12] or targeted therapies in solid tumors.[23-26] Mcl-1-directed therapeutic strategies are particularly promising since *MCL1* is within one of the most frequently amplified chromosomal regions in human cancers making it a high priority therapeutic target.[27] Despite their high target affinities, Mcl-1 inhibitors are generally ineffective as a single agent in most tumors, except those of hematological origin.[28-31] This led to phase 1 clinical trials of several compounds [S64315 (Servier), AMG176 (Amgen) and AZD5991 (AstraZeneca)] currently underway for hematological malignancies.[18] Among Mcl-1 inhibitors, MIM1 (Mcl-1 Inhibitor Molecule 1) (Fig. 1) was identified from a broad screening of more than 70,000 small molecules to find those that could displace a fluorescently labeled Mcl-1 $SAHB_A$ (stabilised α-helix of Bcl-2 domain)[32] from the BH3-binding domain of Mcl-1[33] and not displace a fluorescently labelled Bad-BH3 peptide from the BH3-binding domain of Bcl-x_L. Despite a modest Mcl-1 inhibitor activity with IC_{50} value of 4.8 µM, MIM1 was the first small molecule to exhibit selectivity for Mcl-1 over Bcl-x_L. However, several questions remain. Especially, later studies have indicated that the effects of MIM1 could be cell-line dependent.[34] Moreover, the first SARs provided evidence of specific binding, but did not identify the structural elements of MIM1 that are actually responsible for the observed inhibition.[35] However, cells devoid of the intrinsic apoptosis machinery were unaffected by MIM1, suggesting its cell activity is on-target. Given the modest activity of MIM1, it is envisaged that a Structure–Activity Relationship (SAR) campaign is presently underway toward its optimization.[36]

We started a program around the structure of MIM1 in order to design new and more potent analogues. Indeed, MIM1 caught our attention because we had already performed several studies on polyphenol-type derivatives as inhibitors of the anti-apoptotic protein Bcl-x_L.[37-41] During this study, we realised that the proposed MIM1 structure was not correct. Therefore, we performed extensive NMR, X-Ray crystallography and various physicochemical analyses to revise the structure of the MIM1 molecule from **1** to **2** (Fig. 1).

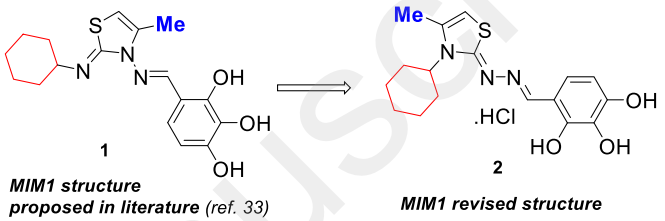

Fig.1 Structures of already published MIM1 **1** and revised structure **2**.

We then designed and synthesised a targeted library of selected new analogues of **2**. These molecules were subjected to appropriate biological studies, examining the pro-apoptotic activity of these molecules in addition to Bcl-x_L or Mcl-1 inhibition, using intact cells to overcome the problems of cellular penetration of the molecules (IGROV1-R10 cell line). These cells have been previously described as dependent on these two anti-apoptotic proteins for their survival, and therefore allow identification and discrimination between Bcl-x_L inhibitors, Mcl-1 inhibitors and dual inhibitors. These studies provided us with preliminary information about the SAR in these series and allowed us to identify two hit molecules, for which Mcl-1 binding affinity was confirmed by fluorescence polarization assay [FPA]. Finally, the SAR obtained with these new MIM1 analogues were rationalised through extensive molecular modelling studies.

Results

1. *Revision of the chemical structure of MIM1*

Since we observed some unexpected results in the physicochemical data of MIM1, we decided to reconsider the synthesis and the structure of this molecule. The literature indicates that the reaction of thiosemicarbazides with α-halogeno ketones has been extensively studied.[42-44] A careful analysis of corresponding data shows that two types of heterocycles were obtained and the heterocyclisation process strongly depends on the structure of the starting thiosemicarbazides, as shown in Scheme 1. In a first step, the

sulphur atom in molecules **3/3'** displaces the bromide from **4** to afford sulfonium ion intermediates **5/5'**. For these compounds, two forms are possible, **5a/5'a** and **5b/5'b**, and for each of them the intramolecular cyclisation by a nitrogen atom, followed by water and HBr elimination, will lead to a different structure: a thiazol-3(2H)-yl)imino core **6/6'** if the nitrogen atom of the hydrazone group is concerned by the cyclisation (pathway 1) or a [2(3*H*)-thiazolylidene]hydrazone **7/7'** if the terminal nitrogen atom is involved (pathway 2).

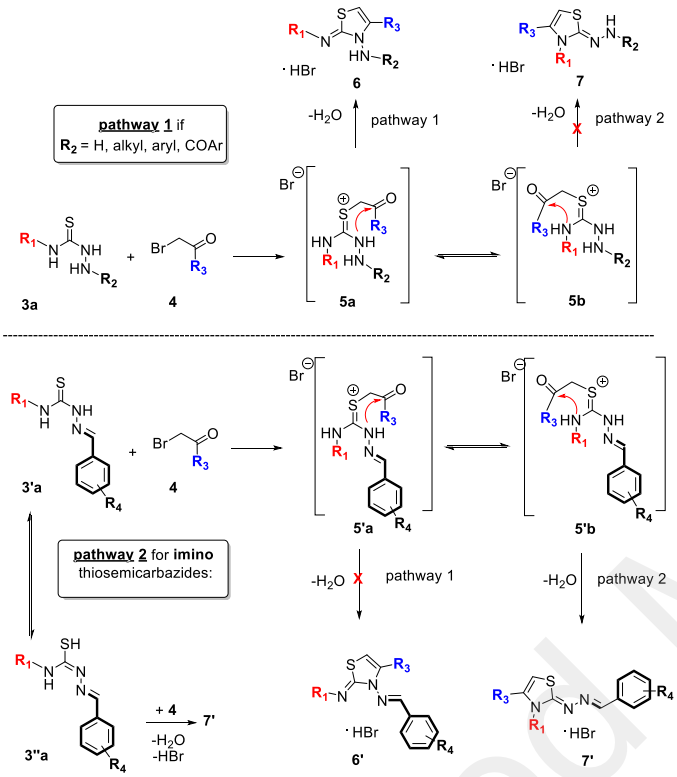

Scheme 1 Two possible pathways for the condensation of thiosemicarbazides with α-halogenoketones

Careful analysis of literature data indicates that the pathway 1 is observed for molecules **3a** in which the amino groups have $\mathbf{R_2}$= H, alkyl or aryl, and also when $\mathbf{R_2}$ is COAr or $COCH_2Ar$ to give compound-types **6**.[45-53]

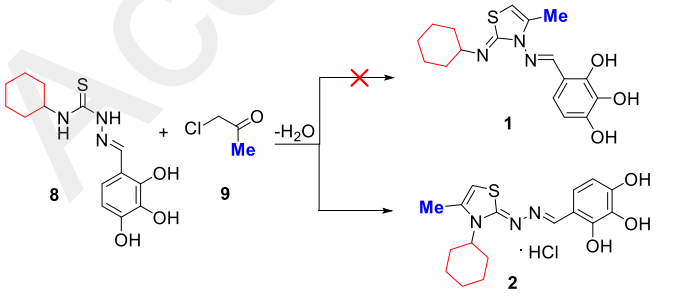

Scheme 2 Synthesis of MIM1 by reaction of the pyrogallol-derived-imino-thiosemicarbazide **8** with α-chloroacetone **9**.

However when an imino-thiosemicarbazide, such as **3'a**, is involved as starting material, the pathway 2 (through **5'b**), is favoured affording compound-types **7'**. Alternatively, it is possible to start the reaction from **3''a**, the tautomeric form of **3'a** with a conjugated diazadienyl thiol structure, leading also to **7'**.[54-62]

The synthesis of compound **1** has been reported by L. D. Walensky *et al.* using this classical method by the reaction of the pyrogallol-containing imino-thiosemicarbazide **8** with chloroacetone **9** (Scheme 2).[33]

The structure **1** proposed by L. D. Walensky *et al.* for MIM1, with a thiazol-3(2*H*)-yl)imino core, implies that the first pathway was involved in that case, while the second pathway leading to the isomeric molecule **2** is occurring in previous literature examples. Therefore, it became important to establish unambiguously the structure of MIM1. The synthesis of this molecule was repeated, following the literature procedure and we obtained a compound with identical physical properties, including NMR data which were matching very well with those reported by L. D. Walensky *et al.*[33] Then, extensive 2D NMR experiments were performed, under appropriate conditions (see experimental section and Supplementary Information: SI) to assign unambiguously all protons and carbon signals of this molecule. Most significant were the NOESY experiments: they showed very clearly strong correlations between the protons of the methyl group and the C**H** and C**H**$_2$ groups of the cyclohexyl unit (see copies of spectra in SI). Such data are clearly incompatible with molecule **1** having a thiazol-3(2H)-yl)imino core, since in that case these groups are in 1,3 position. On the contrary, these two groups are vicinal in the (thiazol-2(3*H*)-ylidene)hydrazineylidene)-type structure **2** and therefore in proper position for strong NOE's correlations. Despite many attempts, it was not possible to obtain crystals of **2** suitable for X-Ray diffraction studies. Therefore, we prepared various analogues and when we performed the same synthesis starting from imino-thiosemicarbazide **10** bearing three methoxy groups, we obtained a compound **11,** similar to **2** with replacement of the phenols by three methoxy groups. The data of **11** were matching perfectly with the structure and in particular, NMR studies gave again strong NOE correlations between the methyl group and the C**H** and C**H**$_2$ groups of the cyclohexyl unit. Further, molecule **11** was analysed by X-Ray diffraction and the crystallographic data confirmed the (thiazol-2(3*H*)-ylidene)hydrazineylidene)-type structure, as indicated in scheme 3, figure 2 and SI. By the same route, we prepared two other derivatives lacking the pyrogallol unit, molecules **14a** and **14b** which could be analysed also by X-Ray diffraction (Scheme 3, Fig 2 and SI) and both of these molecules have also the same (thiazol-2(3*H*)-ylidene)hydrazineylidene) basic type of structure and the same stereochemistry at the C=N exocyclic double bond. Interestingly, all these molecules are isolated as HBr or HCl salts, a point which is often missed in previous papers on this type of molecules and which should result in underestimation of IC_{50} values.

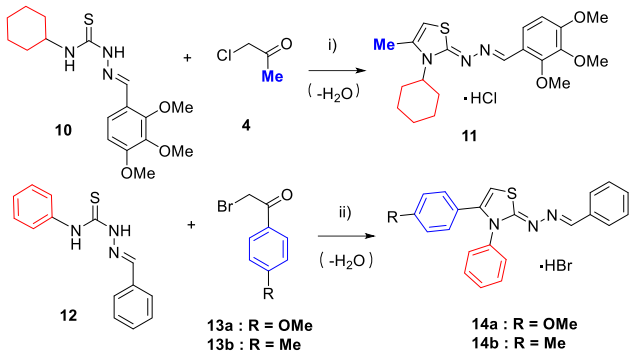

(i) **10** (1.0 mmol), **4** (2.0 mmol) in ethanol/chloroform (7:3) (20 ml) refluxed for 6h **11** : 88% yield ; (i) **12** (1.0 mmol), **13a** (or **13b**) (2.0 mmol) in ethanol/chloroform (7:3) (20 ml) refluxed for 6h **14a** : 78% yield and **14b** : 77% yield.

Scheme 3 Synthesis of compounds **11**, **14a** and **14b** with structures established by X-Ray analysis

Therefore, the structure of MIM1 must be revised from a thiazol-3(2*H*)-yl)imino-type molecule (as in **1**) to a (thiazol-2(3*H*)-ylidene)hydrazineylidene)-type derivative (as in **2**) containing a HCl molecule (Fig. 2).

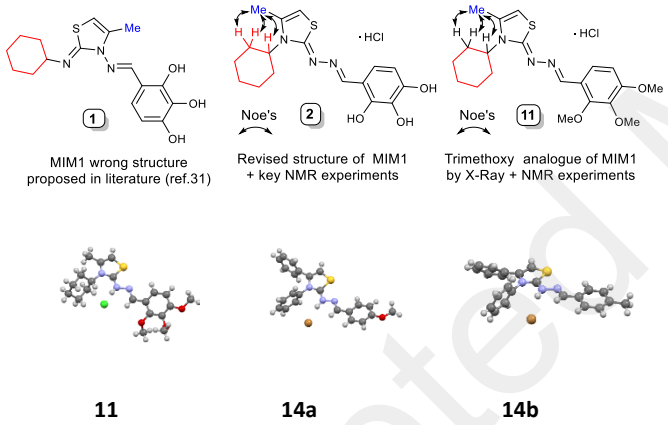

Fig. 2 Revised structure of MIM1 from **1** to **2** with key structural data, plus the structure of **11**, **14a** and **14b** by X-Ray crystallographic analysis.

2. *Design and synthesis of new MIM1 analogues*

Molecular modelling studies, NMR experiments and mutagenesis data indicated that the pyrogallol part of the MIM1 molecule **2** plays a key role to anchor those compounds onto the Mcl-1 protein.[33] Therefore, this part was kept in our studies and we designed a series of analogues to explore the possible effect of the R_1 and R_3 groups on the action of corresponding molecules on the anti-apoptotic proteins Mcl-1 and Bcl-x_L. We kept in mind that this scaffold, as MIM1 itself, bears several substructural features related to frequent hitters or PAINS.[63] However, the results and data presented in the following sections will dispel any concerns about the actual activity of the compounds, e.g. SAR, orthogonal assays and dose-response data (Ki).[64] For these R_1 and R_3 groups, we selected two families of substituents, either phenyl/pyridyl groups or benzyl and pyridymethyl groups. The preparation of these thirteen analogues is described in Scheme 4. The starting thioureas **21** were obtained in a classical manner by reaction of hydrazine hydrate on the corresponding isothiocyanates.[65-67] By reaction with aldehyde **18**, they gave the imino-thiosemicarbazides intermediates **22a**-**22g** in good yields (Table 1).

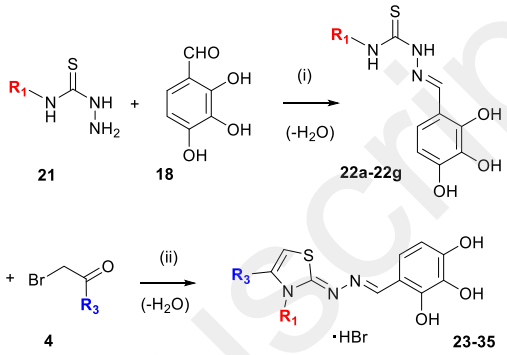

(i) **21** (1.0 mmol), **18** (1.0 mmol) in methanol (15 ml) refluxed for 6h. The yields are given in Table 1 ; (ii) **22** (1.0 mmol), **4** (2.0 mmol) in ethanol/chloroform (7:3) (20 ml) refluxed for 6h. The yields are given in Table 2.

Scheme 4 Synthesis of imino-thiosemicarbazides **22** and selected target molecules **23**-**35**.

Table 1 Synthesis of the imino-thiosemicarbazides **22**

Entry	R_1	Product (Yield %)
1	Ph-	**22a** (82%)
2	$PhCH_2$-	**22b** (77%)
3	4Et-Ph-	**22c** (76%)
4	4Cl-$PhCH_2$-	**22d** (73%)
5	4Et-$PhCH_2$-	**22e** (68%)
6	3Py-	**22f** (74%)
7	3Py-CH_2-	**22g** (78%)

Table 2 Synthesis of the targeted MIM1 analogues **23-35**

Entry	R_1	R_3	Product (Yield %)
1	Ph-	$PhCH_2$-	**23** (49%)
2	3Py-CH_2-	4Py-	**24** (72%)
3	Ph-	4Py-	**25** (52%)
4	$PhCH_2$-	$PhCH_2$-	**26** (55%)
5	$PhCH_2$-	Ph-	**27** (51%)
6	$PhCH_2$-	4Cl-$PhCH_2$-	**28** (81%)
7	4Cl-$PhCH_2$-	Ph-	**29** (55%)
8	4Et-$PhCH_2$-	Ph-	**30** (50%)
9	4Et-Ph	Ph-	**31** (57%)
10	3Py-CH_2-	Ph-	**32** (53%)
11	3Py-	Ph-	**33** (53%)
12	$PhCH_2$-	3Py-	**34** (76%)
13	$PhCH_2$-	4Py-	**35** (74%)

Then reaction of these intermediates with various α-halogeno-ketones **4** afforded in fair to good yields (Table 2) the target molecules **23**-**35**.

3. *Biological studies*

3.1 MIM1 derivatives in vitro screening**.**

3.1.1 Screening models.

The biological activity of these molecules has been evaluated in a cell line previously described[22] (IGROV1-R10) as depending on both Bcl-x_L and Mcl-1 for its survival. Indeed, whereas neither Bcl-x_L nor Mcl-1 inhibition leads to cell death, their concomitant inhibition induces a massive apoptotic cell death. We thus inhibited either Bcl-x_L or Mcl-1 using specific pharmacological inhibitors (ABT-737 for Bcl-x_L and S63845 for Mcl-1) and exposed these cells to the new molecules. The use of this model allows the distinction between Mcl-1 inhibitors, Bcl-x_L inhibitors or dual inhibitors, although our screening results are only indicatives.

3.1.2 MIM1 exerts a modest activity on IGROV1-R10 cell lines.

We first evaluated the effect of MIM1 (compound **2**) on our model, alone or in combination with pharmacological inhibitors (ABT-737 for Bcl-x_L, S63845 for Mcl-1)(Fig. 3). A preliminary study allowed to identify the optimal concentration of each molecule, the association of 5 µM ABT-737 and 1 µM S63845 inducing a massive cell death in IGROV1-R10 whereas neither of these molecules induced cell death when used separately (SI Fig. 5). As expected, 10 µM MIM1 (**2**) did not exert any effect as a single agent. However, the association of 10 µM MIM1 (**2**) with the inhibition of Mcl-1 or Bcl-x_L showed a little activity on our cell line. A modest number of detached cells and few condensed or fragmented nuclei were observed, despite the fact that many sub-G1 events were observable in DNA content histograms, probably more indicative of the presence of small debris than of massive cell death. At 25 µM, a dual effect seems to occur, that could reflect off-target effects as well as dual specificity for the two targets.

To evaluate the efficiency of MIM1 analogues, same experiments than described above were performed and western blot evaluating caspase 3 cleavage was added to our experimental pipeline in order to classify and to quantify effect of each molecule on apoptosis induction based on their activity or selectivity to Mcl-1, Bcl-x_L or both. Moreover, a Python script was executed on DAPI staining to quantify nuclei aspects and evaluate the effect on apoptosis induction. Most of the MIM1 derivatives tested present an improved activity as compared to MIM1 (**2**) since their activity was optimal at 10 µM, a focus on the most representative molecules is presented below. Some of the compounds appeared as completely inactive, even in presence of ABT-737 or S63845. For instance, this is the case of the compound **25**. As an evidence there was no apoptotic induction by these compounds as shown by the low fragmented/total nuclei ratio and the absence of caspase 3 cleavage (Fig. 5 & Fig. 6, grey frame). In addition, no sub-G1 peak is observed under such conditions. Other compounds appeared as dual Bcl-x_L/Mcl-1 inhibitors. Among them, compound **27** appeared as the most potent one, as shown by the strong cell detachment, the high proportion of condensed or fragmented nuclei (and by the high proportion of events in the sub-G1 fraction on DNA content histograms, Fig. 4, blue frame). Caspase 3 cleavage reveal a more potent activity in combination with either ABT-737 or S63845 as compared to MIM1 (**2**) (Fig. 6, blue frame). However, none of them was active as single agent, showing that they were not able to completely inhibit both Bcl-x_L and Mcl-1 and that they require another pharmacological agent targeting one of the two proteins to induce cell death.

Interestingly, other compounds appeared as more specific Mcl-1 inhibitors. As an example, IGROV1-R10 cells exposed to compound **34** in combination with ABT-737, but not with S63845, underwent extensive apoptosis as shown by massive cell detachment and shrinkage, appearance of strong sub-G1 peaks (76.3% and 78.8% respectively) (Fig. 4 orange frame) and numerous nuclear condensations and fragmentations (Fig. 4 & Fig. 5, orange frame). The compound **34** appeared as the most specific and potent Mcl-1 inhibitor of this series.

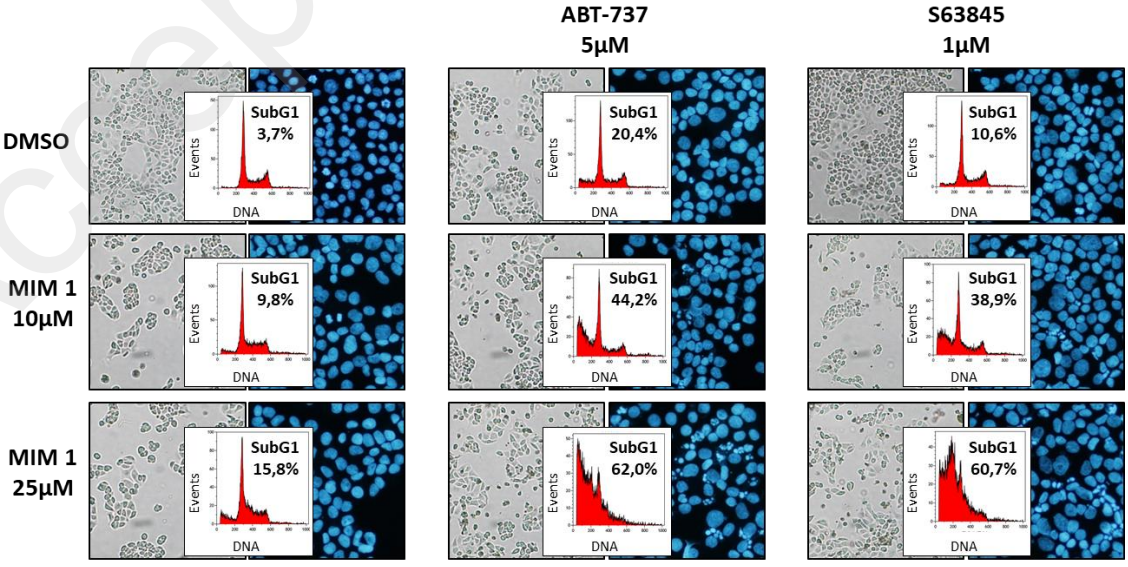

Fig. 3 Effect of MIM1 (**2**) on apoptosis in IGROV1-R10 ovarian cancer cell line after Bcl-x_L or Mcl-1 pharmacological inhibition. Cellular morphology, DNA content and nuclear morphology were assessed in IGROV1-R10 cells exposed to 10 µM or 25 µM MIM1 (**2**) for 24h in combination with either ABT-737 (at 5 µM) to inhibit Bcl-x_L or S63845 (at 1µM) to inhibit Mcl-1.

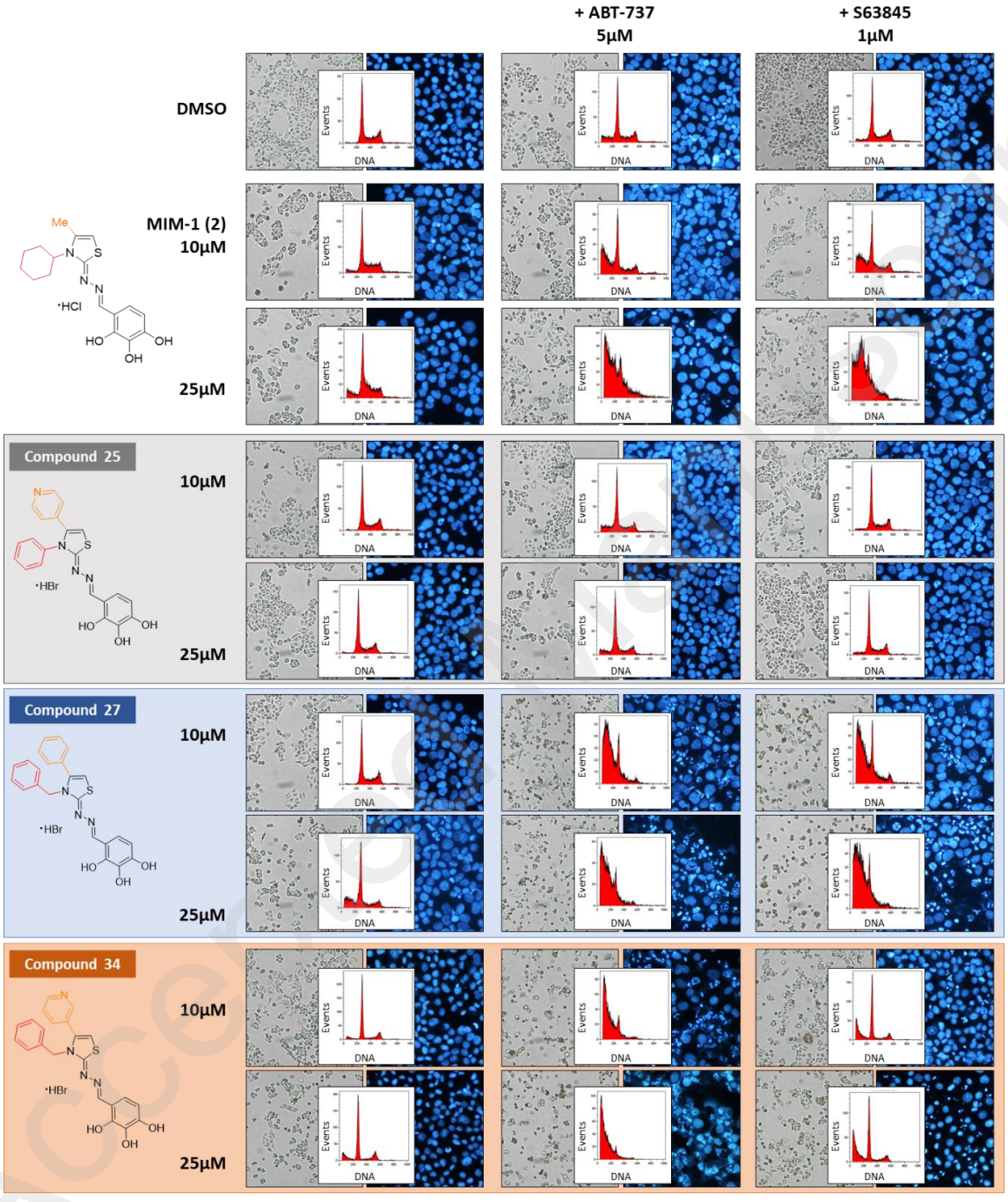

Fig. 4 Effect of MIM1 (**2**) and analogues in combination with Bcl-x_L or Mcl-1 inhibitors on apoptosis in IGROV1-R10 ovarian cancer cell line. Cells were exposed to 10 or 25 µM MIM1 (**2**) or analogues for 24h alone (left panel), in combination with 5 µM ABT-737 (middle panel), or 1 µM S63845 (right panel). Effects on cellular morphology, on DNA content, on nuclear morphology were assessed.

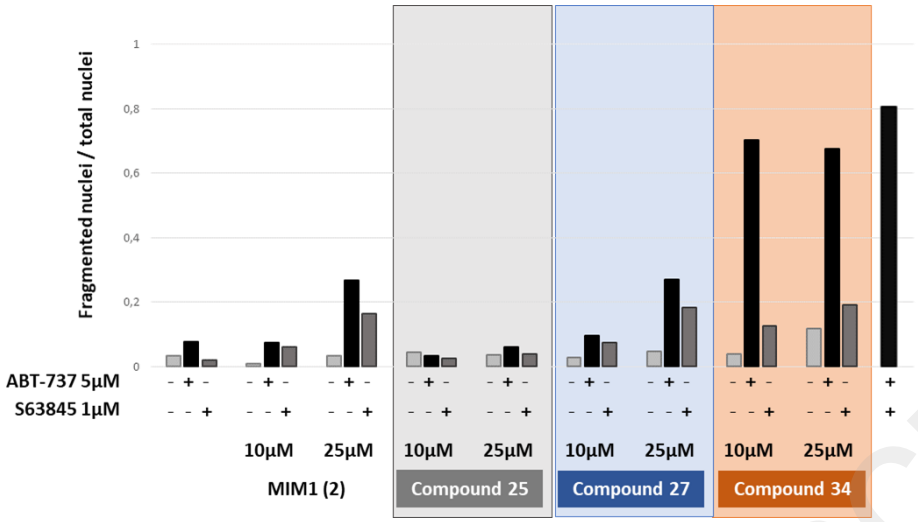

Fig. 5 Effect of MIM1 (**2**) and analogues in combination with Bcl-x_L or Mcl-1 inhibitors on IGROV1-R10 ovarian cancer cell line nuclei. Cells were exposed to 10 µM or 25 µM MIM1 (**2**) or analogues for 24h as single agent, in combination with 5 µM ABT-737, or 1 µM S63845. Effects on nuclear shrinkage and fragmentation were quantified using an automated algorithm.

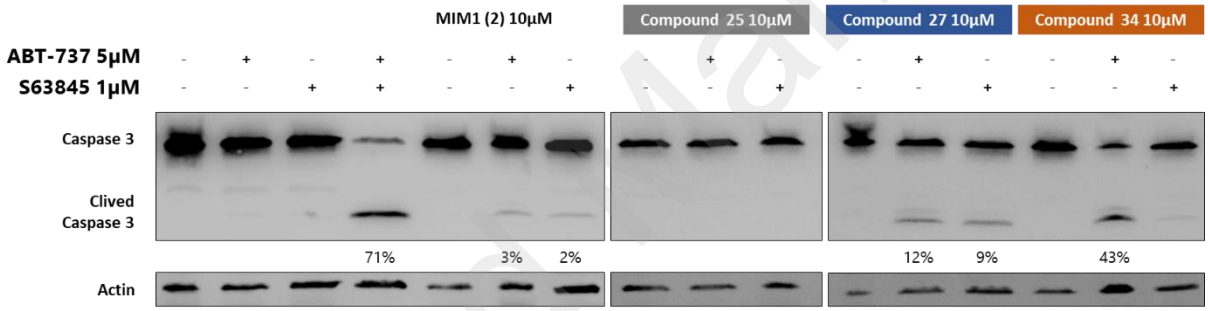

Fig. 6 Effect of MIM1 (**2**) and analogues in combination with Bcl-x_L or Mcl-1 inhibitors on apoptosis in IGROV1-R10 ovarian cancer cell line. Cells were exposed to 10 µM MIM1 (**2**) or analogues for 24h as single agent, in combination with 5 µM ABT-737, or 1 µM S63845. Effects on caspase 3 cleavage were assessed. Percentages represent the ratio of cleaved caspase 3 to the full-length form. Quantification are only indicated below conditions that show a cleaved form high enough to be quantified.

3.2 Fluorescence polarization assays.

In order to demonstrate the capacity of the MIM1 analogues to directly interact with Mcl-1 and to disrupt protein-protein interactions, we measured the binding affinity of our compounds to Mcl-1 *in vitro* by using fluorescence polarization assays (FPA). Briefly, this competition assay investigated the ability of the potential inhibitor to displace a fluorescent-labelled BH3 peptide (we used 5-FAM-Bid) from binding Mcl-1, Bcl-x_L and Bcl-2. By using an unlabelled Mcl-1 BH3 peptide (we used BIM-WT) as positive reference, we determined an IC_{50} (inhibitor concentration at which 50% of labelled peptide is displaced) for several representative compounds (See SI Table 1) and this was converted into a binding dissociation constant (Ki) according to the formula described by Nikolovska-Coleska *et al.*[68] (more details in experimental section).

Binding affinities are presented in Table 3. As expected, dual inhibitors (compound **27**) as well as Mcl-1 specific inhibitors (compound **34**) showed the capacity to efficiently disrupt Mcl-1/5-FAM-Bid interaction in a similar manner (1 µM<Ki<5 µM), suggesting that biological activities are related to an "on-target" effect. In contrast, compound **25** displayed low affinity (Ki>40 µM) in the same experimental conditions.

Table 3. Binding affinities of MIM1 (**2**) and some MIM1 analogues with Mcl-1.

Entry	Compound	R_1	R_3	Mcl-1[a] *Ki* (μM)
1	**2**[b]	*c*-hex-	Me-	2.6[c]
2	**25**	Ph-	4Py-	43.4
3	**27**	$PhCH_2$-	Ph-	3.9
4	**30**	4Et-$PhCH_2$-	Ph-	4.5
5	**31**	4Et-Ph	Ph-	3.5
6	**32**	3Py-CH_2-	Ph-	4.9
7	**34**	$PhCH_2$-	3Py-	4.1
8	**35**	$PhCH_2$-	4Py-	1.1

[a]Ki values were measured in duplicate; [b]revised MIM1; [c]Ki value is comparable to others found in the literature.[33]

3.3 SAR studies

From a structural point of view, our analogues can be classified into four series, depending upon the nature of substituents R_1 and R_3 linked to the cyclic nitrogen atom and to the vicinal carbon on the heterocycle (Fig. 7). For instance, in the series 1 two phenyl/benzyl groups were added while the series 2 had only benzyl substituents. Then the series 3 has aryl and pyridyl groups, while the series 4 has combinations of one phenyl or pyridyl substituent with one benzyl or pyridylmethyl group. The key biological results are summarised in Figure 7, indicating in a schematic manner the activity and selectivity of these molecules on both Mcl-1 and Bcl-x_L anti-apoptotic proteins.

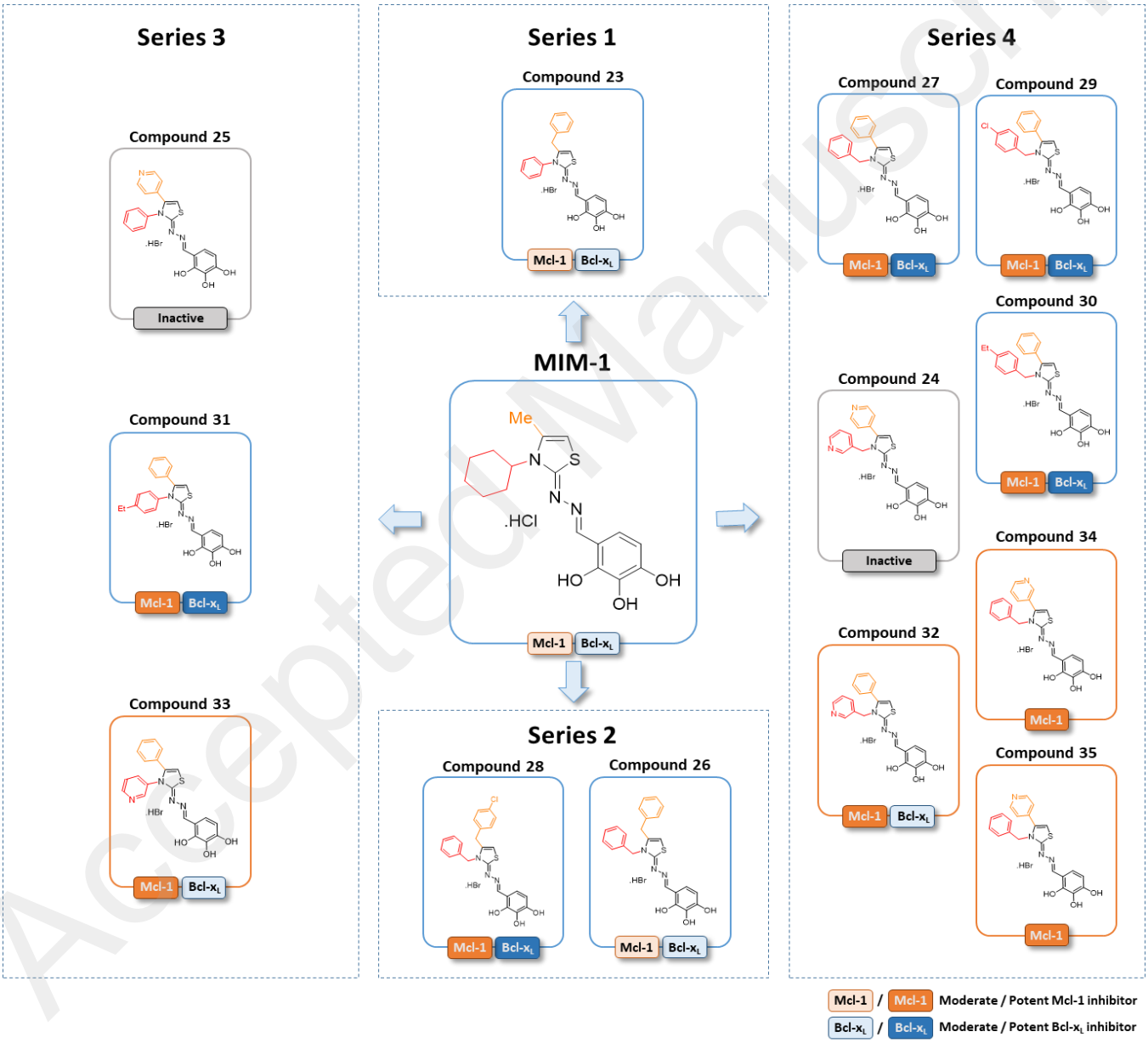

Fig. 7 Schematic analysis of the biological activity in MIM1 series.

From these data it appears clearly that, even if some active compounds were identified in the other series, the series 4 is the most interesting. Indeed, it has the most potent compounds, both in terms of dual inhibitors (**27**, **29** and **30**) as well as for selective Mcl-1 inhibitors (**34** and **35**). It includes also an inactive molecule (**24**). Therefore, we focused on this family of analogues to discuss the SAR of corresponding molecules.

4 SAR in the light of molecular modelling studies

In the original work, experimental data (NMR as well as mutagenesis) showed that M231 and L235 of Mcl-1 belonged to the binding site of MIM1. In addition, docking experiment suggested that V253, D256 and R263 could also be involved in ligand recognition. We reproduced well the proposed binding mode using the initial proposed structure of MIM1 (**1**). Using the same docking parameters, the binding mode of the revised MIM1 (**2**) did not change greatly (Fig. 8A).

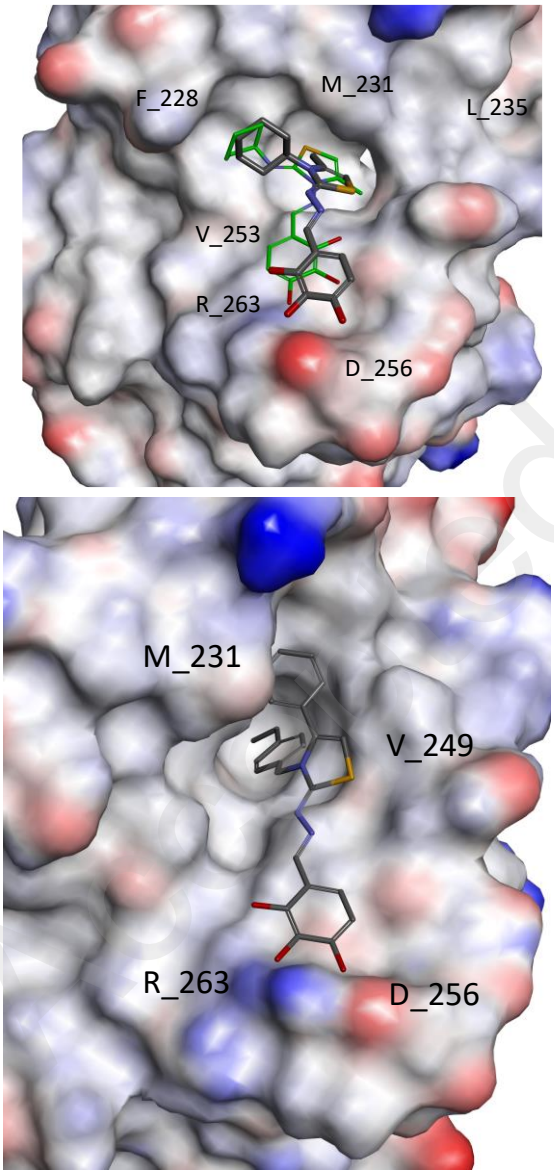

Fig. 8 (A) (up) Superposition of proposed binding mode of the initial MIM1 structure **1** in Mcl-1 (thin bonds with carbon atoms in green), and the revised formula **2** (thick bonds with atoms carbon in grey). (B) (down) Proposed binding mode of **30** in Mcl-1.

The triphenol is still engaged in hydrogen bonds with D256/R263, the thiazole is still in the middle of the crevice, sandwiched between M231 and V253, and the cyclohexyl group forms van der Waals interactions with F228 and the alkyl chains of T266. As the previously supposed structure, the revised MIM1 (**2**) is still too distant for a direct interaction with L235 (10 Å). However, this residue should be important to restrict the conformational freedom of the neighbouring M231, which explains its involvement in ligand affinity.

In Mcl-1, the novel derivatives we synthesised in this study show a similar binding mode to MIM1 (**2**). The main difference is that the addition of a second bulky group caused a flip of the ligand in the binding site. The new phenyl group in position 3 or 4 of the thiazole opens the cavity located underneath M231. The cycle is buried around F270, V249 and L267, within a cavity that extends up to L186, L290, L246 and I294. Only alkyl amino acids are present here, and the strong hydrophobicity of the cavity explains the preference for hydrophobic substituents of the thiazole.

For example, the ethyl-benzyl in position 3 of **30** is swallowed in the deep cavity, packed with F270 and resulting in π-stacking, while the phenyl in position 4 shows extensive van der Waals interactions with an open pocket bordered by M231 and V249, facing R263/D256 (Fig. 8B). Surprisingly, a more polar group is tolerated on the thiazole position 3 of **32**. In fact, the flexibility of M231 allows again a flip of the ligand in order to bury the most hydrophobic part. Consequently, the pyridine is expelled and becomes solvent-exposed. Hence docking of **32** suggests an engulfment of the 4-phenyl in the deep cavity, while the pyridine in position 3 occupies this time the open pocket (Fig. 9A). Although the pyridine cannot find here a residue to form direct hydrogen bond with, a water-bridged interaction might link it to M231 or F228 amide backbone. If the pyridine is on the position 4 (**35**), a small sliding of the ligand permits engulfment of the 3-benzyl in the deep cavity, while the pyridine in position 4 occupies the open pocket (Fig. 9B). However, if the ligand bears two hydrophilic groups, the affinity drops (**24**). In that case, either the second pyridine is expelled from the deep cavity, or it occupies it, but at the cost of the high desolvation energy of a pyridine. Since there is no hydrogen bond possibility with the protein here, the desolvation cost associated with the binding of pyridine is prohibitive (the desolvation energy is 0.9 kcal/mol for a benzene, 4.7 kcal/mol for a pyridine).[69]

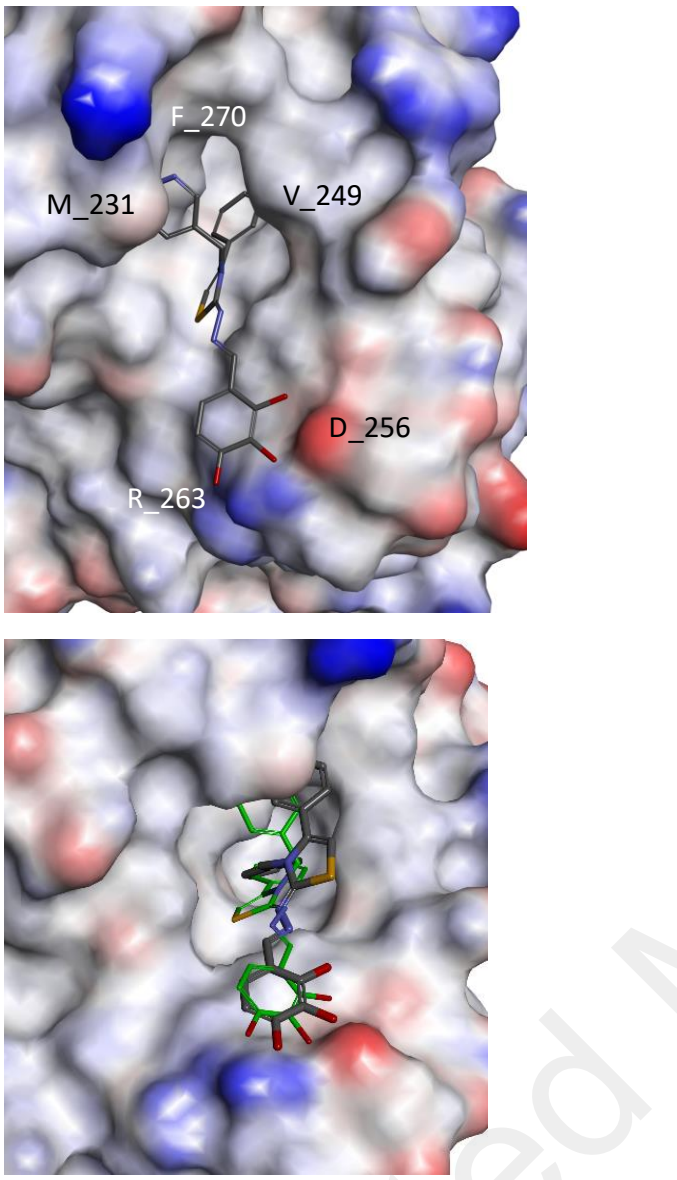

Fig. 9 (A) (up) Proposed binding mode of **32** in Mcl-1. (B) (down) Superimposition of **32** (thin bonds with carbon atoms in green), and **35** (thick bonds with atoms carbon in grey) in Mcl-1.

For Bcl-x_L, docking and computational studies suggested that **30** is bounded in a cavity surrounded by R139, D133, Y101, L108 and V126 (For details, see SI). The triphenol forms extensive hydrogen bonds with ionic pairs R139/D133 and/or R132/E129 (SI Fig. 7A). The thiazole is above V126, while the phenyl interacts with L108, V126 and L112, overhangs by Q111. The ethyl-benzyl is buried in the deep cavity, interacting with F146, L108, A104, Y101 and F97. As already observed for Mcl-1, the ligand is able to flip in the binding site in order to minimise the solvent exposition of most hydrophobic parts. Hence the most enclosed cavity binds either position 3 of the thiazole (**30**), or position 4 (**32**, SI Fig. 7B).

However, the pronounced curvature of Bcl-x_L crevice renders it more hydrophobic than Mcl-1 (Fig. 10). This topological property forces ligands to be more desolvated than for Mcl-1, and hydrophilic groups, such as pyridines, are more penalised within Bcl-x_L binding site. This was confirmed by molecular dynamics, showing that **35** is more solvated in Mcl-1 binding site than is Bcl-x_L, (SI Fig. 8) and explaining why **35** is selective for Mcl-1 in spite of a similar binding mode in both proteins.

Discussion

Biological results obtained on IGROV1-R10 ovarian cancer cell line showed that MIM1 (**2**) does not display a strong cytotoxic activity on these cells as compared to the previously published results obtained on cell death in MCL-1-dependent leukemia cells.[33] Nevertheless, when used at 10 µM, MIM1 (**2**) associated with Bcl-x_L or Mcl-1 pharmacological inhibitors was able to induce a small amount of sub-G1 events. However, the observed effect at 10 µM is mainly cytostatic and only a modest apoptotic cell death level was detected when 25 µM MIM1 (**2**) was associated with ABT-737 as well as with S63845. In agreement with a previous study that showed that MIM1 (**2**) failed to induce apoptosis in two Mcl-1-dependent non-small cell lung carcinoma cell lines,[34] MIM1 (**2**) did not exert any cytotoxic activity even at the higher concentration used (25 µM) in A2780 ovarian cancer cells (data not shown), previously described as highly dependent on Mcl-1 for their survival. It should be noticed that in A2780 cancer cells, Mcl-1 expression level is very high and that our previous studies showed that a higher amount of siRNA and or pharmacological inhibitors are required to lead to efficient Mcl-1 inhibition and subsequent cell death.[22] Otherwise, such a relative resistance of ovarian cancer cells as compared to other cancer cell types to anticancer agents is commonly admitted.

In a drug design approach, some chemical modifications of MIM1 structure led to a complete loss of activity (compounds **24** and **25**). This was observed when a polar group such as pyridine was present instead of a benzyl substituent, without inner flexibility of the ligand to allow a readjustment in the binding site.

Interestingly, MIM1 chemical modifications also led to molecules showing an increased activity as compared to MIM1 (**2**). Compounds **34** and **35** were the most potent and specific Mcl-1 inhibitors, resulting from a perfect fit of the benzyl in the strongly hydrophobic cavity. A massive apoptotic cell death was induced by these molecules (from 5 µM) in combination with ABT-737, whereas MIM1 (**2**) did not exert any effect in these conditions. FPA results are globally in adequacy with all these biological observations identifying consistent binding affinities.

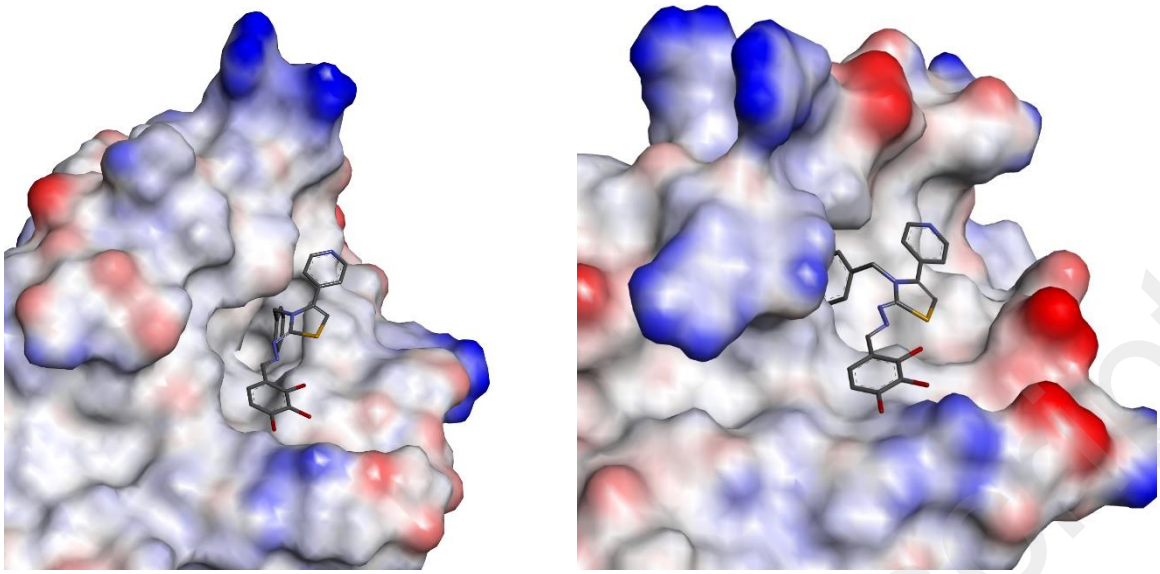

Fig. 10 Compound **35** docked onto Mcl-1 (left) and Bcl-x_L (right). One can observe that the pyridine is much more solvent-exposed in the former.

Conclusions

In summary, after revision of the structure of MIM1 to compound **2**, we have prepared a chemical library of designed analogues of the corrected molecule. Detailed biological studies using IGROV1-R10 ovarian chemoresistant cell line allowed us to discover derivatives which are more potent Mcl-1 inhibitors, as shown by their capacity to induce cell death in combination to Bxl-x_L inhibitors in our model. Substitution of the aromatic group by a pyridine conferred a high selectivity for Mcl-1 vs. Bxl-x_L, especially when this pyridine is in position 4 of the thiazole.

In cellulo results are globally consistent with the capacity of the compounds to bind to Mcl-1 and to inhibit its ability to sequester its pro-apoptotic partner, as determined by the FPA binding assays. All these data gave us a preliminary SAR for the most attractive new MIM1 analogues able to inhibit Mcl-1. Extensive computational studies allowed us to propose a rationale to this SAR, highlighting the role of the polyphenol moiety to anchor these molecules to the binding site and the position of the aromatic/benzyl groups inside the hydrophobic pocket. Regarding the selectivity between Mcl-1 and Bcl-x_L, we found that the global shape of the grooves (more open in Mcl-1 and narrower for Bcl-x_L) appears to play an important role, especially when inhibitors contained polar groups. In the latter case, desolvation processes drove the selectivity of inhibitors towards anti-apoptotic proteins.

EXPERIMENTAL PROCEDURES

Chemical synthesis and analysis

General informations: NMR spectra were performed on a Bruker AVANCE 300, AVANCE 400 or Bruker AVANCE 500 (^{1}H at 400, 300 MHz or 500 MHz; ^{13}C at 75 MHz, 101 or 126 MHz). Solvent peaks were used as reference values with $CDCl_3$ at 7.26 ppm for ^{1}H NMR and 77.16 ppm for ^{13}C NMR, with MeOD at 4.78 and 3.31 ppm for ^{1}H NMR and 49.00 ppm for ^{13}C NMR, with DMSO-d_6 at 2.50 and 3.33 ppm for ^{1}H NMR and 39.52 ppm for ^{13}C NMR, and with DMF-d7 at 8.03, 2.92 and 2.75 ppm for ^{1}H NMR and 163.15, 24.89 and 29.76 ppm for ^{13}C NMR. Chemical shifts δ are given in ppm, and the following abbreviations are used: singlet (s), broad singlet (bs), doublet (d), doublet of doublet (dd), doublet of doublet of doublet (ddd), triplet (t), triplet of doublet (td), quadruplet (q), doublet of quadruplet (dq), and multiplet (m). Non Uniform Sampling (NUS) acquisition methods for multidimensional NMR within topspin were run to complete conventional measurements, which is uniformly sampled (US). The goal of NUS is to improve spectral resolution obtained in a given amount of measurement time to get a full set of ^{13}C peaks when conventional 2D experiments fail to. (HSQC, HMBC were respectively ran with 25 and 50% of NUS).

All analogues of MIM1 compounds synthesised are hydrobromide or hydrochloride salts and melting point measured in °C were related to decomposition process. Above a critical concentration [product] > 30 mg/mL in DMSO-d_6 solutions degradation occurred with time. At first without explanation, we discovered later on that DMSO-d_6 reacted with hydrobromide salts to form a strong reagent which react at the H-ethylenic position of the cycle. This observation was also reported in 2015 as a new method for bromination of olefins.[70] Furthermore, hydrobromides salts were completely dissolved with 1 to 4 drops of D_2O added in MeOD-d_4 before ^{1}H and ^{13}C NMR analyses of MIM1 analogues compounds.

IR spectra were recorded on a Perkin Elmer (Spectrum 2) apparatus using a Universal ATR Sampling Accessory and spectra were analysed with spectragryph 1,2,4 version. High resolution mass spectra were recorded in the Centre Régional

de Mesures Physiques de l'Ouest, Rennes (CRMPO), on a Maxis 4G. Microanalyses were performed at CRMPO Rennes on a Thermo-Finigan Flash EA 1112 CHNS/O analyzer. Melting points were determined with uncertainty of ± 2 °C using a KOFLER BENCH. Reaction courses and product mixtures were routinely monitored by TLC on silica gel (precoated F254 Merck plates), and compounds were visualised under a UVP Mineralight UVGL-58 lamp (254 nm) and with *p*-anisaldehyde/Δ. Column chromatography was performed using silica gel 60 (40−63 mm, 230−400 mesh). Solvents were used as received from commercial sources. Reagents were purchased from Sigma-Aldrich, Alfa Aesar and Acros. All corresponding products showed ^{1}H, and ^{13}C NMR spectra in agreement with the assigned structures.

The purity of the samples subjected to biological testing has been established by HPLC analysis and all corresponding molecules had purities >95%. For these analyses, the compounds were solubilised in MeOH/H_2O solution and filtered through 0.45 mm nylon syringe filters prior to injecting a 10 µL aliquot to the HPLC-DAD device. The HPLC analyses were performed on a Prominence Shimadzu HPLC system (Marne La Vallée, France) equipped with a Kinetex C_{18} HPLC column (100 × 4.6 mm, 2.6 µm, 6A, Phenomenex), thermostated at 40°C and including an autosampler (SIL-20AHT), a binary gradient pumping system (LC-20ADSP-PUMP) and a diode array detector (SPD-M20A), with analysis at 365nm. For elution a gradient system was applied using A (water) and B (acetonitrile). The following gradient was applied at a flow rate of 1 ml/min: initial: 20% B to 100% B in linear mode during 20min, then from 100% B to 10% B in linear mode during 20 min, and finally 10% B during 30 min.

General procedure for the synthesis of thiosemicarbazide intermediate [21]

The appropriate isothiocyanate (15.0 mmol) in 15 ml methanol and hydrazine hydrate (90.0 mmol) in 15 ml methanol were mixed and the resulting solution was stirred for one hour. The powder product, the thiosemicarbazide formed was filtered, washed with water, methanol and dried in vacuo. The product was pure enough, based on ^{1}H NMR analyses, to be used in the next step without further purification. For all known compounds (**21a** to **21d** and **21f**-**21g**), their physical and spectral data agreed with the literature.[71, 72]

Hydrazinecarbothioamide, N-[(4-ethylphenyl)methyl] (**21e**)
The reaction was performed with 1-ethyl-4-isothiocyanato methyl-benzene (990 mg, 5.59 mmol) and hydrazine hydrate (1.05 ml, 33.54 mmol), according to the general procedure. The product **21e** was obtained as colorless powder (1.03 g, 88% yield). Mp = 152 °C. ^{1}H NMR (300 MHz, DMSO-d_6): δ 8.70 (s, 1H), 8.20 (bs, 1H); 7.22 (d, 2H, J = 8.0 Hz), 7.13 (d, 2H, J = 8.0 Hz), 4.67 (d, 2H, J = 6.0 Hz), 4,42 (s, 2H); 2.56 (q, 2H, J = 7.6 Hz), 1.16 (t, 3H, J = 7.6 Hz). ^{13}C NMR (75 MHz, DMSO-d_6): δ 181.5, 142.1, 136.7, 127.3 (2C), 127.2 (2C), 45.9, 27.7, 15.6. HRMS (ESI): calcd for $C_{10}H_{15}N_3SNa$: $[M + Na]^+$: m/z 232.08789. Found: m/z 232.0880 (0 ppm).

General procedure for the synthesis of intermediates [22]

A methanolic (20 ml) solution of thiosemicarbazide (1.0 mmol) was added to a solution of 2,3,4-trihydroxybenzaldehyde (**18**) (1.0 mmol) in 15 ml methanol and the reaction mixture was refluxed for 6 h. The product formed was filtered, washed with methanol and dried in vacuo.

Hydrazinecarbothioamide, 2-[(2,3,4-trihydroxy-phenyl) methylene]-N-phenyl (22a)
The reaction was performed with 4-phenylthiosemicarbazide (**21a**) **(**344 mg, 2.06 mmol) and 2,3,4-Trihydroxy-benzaldehyde (**18**) **(**317 mg, 2.06 mmol), according to the general procedure. The product **22a** was obtained as yellow solid (537 mg, 82% yield). Mp = 196 °C. (litt 206°C).[72] ^{1}H NMR (300 MHz, DMSO-d_6): δ 8.66 (s, 1H), 7.59 – 7.18 (m, 5H), 6.98 (d, *J* = 8.4 Hz, 1H), 6.47 (d, *J* = 8.5 Hz, 1H). ^{13}C NMR (75 MHz, DMSO-d_6): δ 175.2, 148.5, 146.8, 142.4, 139.2, 132.8, 128.1, 125.4, 125.0, 118.6, 112.5, 107.8.

Hydrazinecarbothioamide, 2-[(2,3,4-trihydrox-phenyl methyl ene] N-[(phenyl)methyl] (22b)
The reaction was performed with hydrazinecarbothioamide, N-[(phenyl)methyl] (**21e**) (258 mg, 1.42 mmol) and 2,3,4-Trihydroxy-benzaldehyde (**18**) (220 mg, 1.42 mmol), according to the general procedure. The product **22b** was obtained as yellow solid (348 mg, 77% yield). Mp = 212 °C. ^{1}H NMR (300 MHz, DMSO-d_6): δ 11.32 (s, 1H), 9.58 (s, 1H), 8.60 (bs, 3H), 8.27 (s, 1H), 7.33-7.22 (m, 5H), 7.15 (d, 1H, *J* = 8.3 Hz), 6.34 (d, 1H, *J* = 8.3 Hz), 4.81 (d, 2H, *J* = 3.5 Hz).^{13}C NMR (75 MHz, DMSO-d_6): δ 177.0, 148.3, 146.6, 142.2, 139.6, 132.8, 128.2 (2C), 127.3 (2C), 126.7, 118.3, 112.6, 107.7, 48.7. HRMS (ESI): calcd for $C_{15}H_{15}N_3O_3SNa$: $[M + Na]^+$: *m/z* 340.07318. Found: *m/z* 340.0732 (0 ppm).

Hydrazinecarbothioamide, 2-[(2,3,4-trihydroxy-phenyl) methy lene]-N-(4-ethylphenyl) (22c)
The reaction was performed with hydrazinecarbothioamide, N-(4-ethylphenyl) (**21c**) (268 mg, 1.37 mmol) and 2,3,4-Trihydroxy-benzaldehyde (**18**) (212 mg, 1.37 mmol), according to the general procedure. The product **22c** was obtained as yellow solid (346 mg, 76% yield). Mp = 204 °C. 1H NMR (300 MHz, Methanol-d4): δ 8.19 (s, 1H), 7.44 (d, 2H, J = 8.4 Hz), 7.19 (d, 2H, J = 8.4 Hz), 6.95 (d, 1H, J = 8.6 Hz), 6.43 (d, 1H, J = 8.6 Hz), 2.64 (q, 2H, J = 7.6 Hz), 1.23 (t, 3H, J = 7.6 Hz). 13C NMR (75 MHz, Methanol-d4): δ 177.5, 150.0, 147.8, 147.4, 143.3, 137.9, 134.1, 128.9 (2C), 126.5 (2C), 122.1, 113.1, 109.1, 29.4, 16.1. HRMS (ESI): calcd for $C_{16}H_{17}N_3O_3SNa$: [M + Na]+: m/z 354.12223. Found: m/z 354.1223 (0 ppm).

Hydrazinecarbothioamide, 2-[(2,3,4-trihydroxy-phenyl) methy lene]-N-[(4-chlorophenyl)methyl]) (22d)
The reaction was performed with hydrazinecarbothioamide, N-[(4-chlorophenyl)methyl] (**21d**) (267 mg, 1.24 mmol) and 2,3,4-trihydroxy-benzaldehyde (**18**) (191 mg, 1.24 mmol), according to the general procedure. The product **22d** was obtained as yellow solid (318 mg, 73% yield). Mp = 202 °C. ^{1}H NMR (300 MHz, DMSO-d_6): δ 11.36 (s, 1H), 8.87 (t, 1H, *J* = 6.0 Hz), 8.27 (s, 1H), 7.39-7.33 (m, 4H), 7.17 (d, 1H, *J* = 8.6 Hz), 6.34 (d, 1H, *J* = 8.6 Hz), 4.78 (d, 2H, *J* = 6.2 Hz). ^{13}C NMR (75 MHz, DMSO-d_6) δ

176.9, 148.3, 146.6, 142.1, 138.7, 132.7, 131.2, 129.1 (2C), 128.1 (2C), 118.2, 112.6, 107.7, 45.9. HRMS (ESI): calcd for $C_{15}H_{14}ClN_3O_3SNa$: [M + Na]$^+$: *m/z* 374.03421. Found: *m/z* 374.0344 (0 ppm).

Hydrazinecarbothioamide, 2-[(2,3,4-trihydroxy-phenyl) methy lene]-N-[(4-ethylphenyl)methyl] (22e)

The reaction was performed with hydrazinecarbothioamide, N-[(4-ethylphenyl)methyl] (**21e**) (276 mg, 1.32 mmol) and 2,3,4-Trihydroxy-benzaldehyde (**18**) (203 mg, 1.32 mmol), according to the general procedure. The product **22e** was obtained as yellow solid (309 mg, 68% yield). Mp = 196 °C. ^{1}H NMR (300 MHz, DMSO-d_6): δ 11.29 (s, 1H, NH), 9.58 (br, 1H, OH), 8,99 (1H, OH), 8.87 (t, 1H, *J* = 6.0 Hz, NH), 8.44 (br, 1H, OH), 8.27 (s, 1H, Himine), 7.23 (d, *J* = 8.6 Hz, 2Har), 7.17-7.13 (d, 3H, *J* = 8.6 Hz, 2Har + HAr), 6.34 (d, 1H, *J* = 8.6 Hz), 4.78 (d, 2H, *J* = 6.2 Hz), 2.56 (q, 2H, *J* = 8.0 Hz, CH_2), 1.14 (t, 2H, *J* = 8.0 Hz, CH_3). ^{13}C NMR (75 MHz, DMSO-d_6): δ 176.8, 148.3, 146.5, 142.3, 142.0, 136.9, 132.8, 131.2, 127.6 (2C), 127.4 (2C), 118.2, 112.6, 107.7, 45.9. HRMS (ESI): calcd for $C_{17}H_{19}N_3O_3SNa$: [M + Na]$^+$: *m/z* 368.10448. Found: *m/z* 368.1047 (1 ppm).

Hydrazinecarbothioamide, 2-[(2,3,4-trihydroxy-phenyl) methy lene]-N-(3-pyridinyl) (22f)

The reaction was performed with hydrazinecarbothioamide, *N*-3-pyridyl (**21a**) (320 mg, 1.90 mmol) and 2,3,4-trihydroxy-benzaldehyde (**18**) (293 mg, 1.90 mmol), according to the general procedure. The product **22f** was obtained as yellow solid (428 mg, 74% yield). Mp = 250 °C. ^{1}H NMR (300 MHz, DMSO-d_6) δ 11.78 (s, 1H), 10.07 (s, 1H), 9.66 (bs, 1H), 9.07 (bs, 1H), 8.69 (s, 1H), 8.53 (bs, 1H), 8.39 (s, 1H), 8.36 (d, 1H, *J* = 4.3 Hz), 7.99 (d, 1H, *J* = 8.2 Hz), 7.39 (dd, 1H, *J* = 8.0 Hz, *J* = 4.7 Hz), 7.33 (d, 1H, *J* = 8.0 Hz), 6.38 (d, 1H, *J* = 8.6 Hz). ^{13}C NMR (75 MHz, DMSO-d_6): δ 175.7, 148.6, 146.8, 146.7, 145.6, 143.1, 136.1, 132.9, 132.8, 122.8, 118.6, 112.4, 107.8. HRMS (ESI): calcd for $C_{13}H_{12}N_4O_3SNa$: [M + Na]$^+$: *m/z* 327.05223. Found: *m/z* 327.0523 (0 ppm).

Hydrazinecarbothioamide, 2-[(2,3,4-trihydroxy-phenyl) methy lene]-N-[(3-pyridinyl)methyl] (22g)

The reaction was performed with hydrazinecarbothioamide, N-(3-pyridinylmethyl) (**21g**) (218 mg, 1.12 mmol) and 2,3,4-trihydroxy-benzaldehyde (**18**) (184 mg, 1.12 mmol), according to the general procedure. The product **22g** was obtained as yellow solid (281 mg, 78% yield). Mp = 246 °C. ^{1}H NMR (300 MHz, DMSO-d_6): δ 10.41 (s, 1H), 8.63 (s, 1H), 8.03 (s, 1H), 7.94 (t, 1H, *J* = 6.0 Hz), 7.57-7.45 (m, 3H), 7.29 (s, 1H), 6.79-6.75 (m, 1H), 6.36 (dd, 1H, *J* = 7.3 Hz, *J* = 4.8 Hz), 6.19 (d, 1H, *J* = 8.6 Hz), 5.36 (d, 1H, *J* = 8.6 Hz), 3.84 (d, 2H, *J* = 6.1 Hz). ^{13}C NMR (75 MHz, DMSO-d_6): δ 176.9, 148.8; 148.3, 147.9, 146.6, 142.2, 135.2, 135.2, 132.8, 123.5, 118.2, 112.6, 107.7, 44.3. HRMS (ESI): calcd for $C_{14}H_{14}N_4O_3SNa$: [M + Na]$^+$: *m/z* 341.06843. Found: *m/z* 341.0684 (0 ppm).

General procedure for the synthesis of final products [23-35]

A mixture of the appropriate thiosemicarbazide (**22a**-**22g**) (1.0 mmol) and α-halogenoketone (2.0 mmol) in ethanol-chloroform (7:3) mixture (20 ml) was refluxed for 6 h. Then, the mixture was concentrated to ¼ of its volume with precipitation of the product. After cooling at 0°C the filtrate was discarded by canula and the remained precipitate washed several times with cold methanol and diethyl ether using canula filtration between each wash. Then, the powder was dried under vacuum to give the desired product.

4-((*E*)-(((*Z*)-4-benzyl-3-phenylthiazol-2(3H)-ylidene)hydrazine ylidene)methyl)benzene-1,2,3-triol, hydrobromide (23)

The reaction was performed with **22a** (219 mg, 0.72 mmol) and 1-bromo-3-phenyl-propan-2-one (305 mg, 1.45 mmol) according to the general procedure. The product **23** was obtained as solid (175 mg, 49% yield), crystallised from acetone. Mp = 242 °C. ^{1}H NMR (300 MHz, DMSO-d_6): 8.37 (s, 1H), 7.53-7.46 (m, 3H), 7.36-7.33 (m, 2H), 7.22-7.18 (m, 3H), 6.92 (dd, 2H, *J* = 7.2, 2.6 Hz), 6.84 (d, 1H, *J* = 8.6 Hz), 5.51 (s, 1H), 6.39 (d, 1H, *J* = 8.5 Hz), 3.61 (s, 2H). ^{1}H NMR (300 MHz, DMSO-d_6): δ 8.37 (s, 1H), 7.55 – 7.46 (m, 3H), 7.41 – 7.30 (m, 2H), 7.23 – 7.15 (m, 3H), 6.97 – 6.89 (m, 1H), 6.85 (d, *J* = 8.5 Hz,1H), 6.51(s, 1H), 6.39 (d, *J* = 8.5 Hz, 1H), 3.61(s, 2H). ^{13}C NMR (126 MHz, DMSO-d_6) δ 168.2, 152.0, 149.3, 147.7, 140.7, 135.7, 134.4, 132.8, 130.3, 130.0, 128.7, 128.7, 128.5, 126.9, 119.0, 111.5, 108.2, 103.2, 33.7. (30.9 acetone impurity). HRMS (ESI): calcd for $C_{23}H_{19}N_3O_3SNa$: [M + Na]$^+$: *m/z* 440.10393. Found: *m/z* 440.1037 (0 ppm). HPLC analysis, compound **23**: t_R = 15.3 min; purity: 99.4 %.

4-((*E*)-(((*Z*)-4-(pyridin-4-yl)-3-(pyridin-4-ylmethyl)thiazol-2(3H)-ylidene)hydrazineylidene)methyl)benzene-1,2,3-triol, hydrobromide (24)

The reaction was performed with **22f** (79 mg, 0.25 mmol, 1.0 equiv.) and 4-(bromoacetyl)pyridine hydrobromide (70 mg, 0.25 mmol, 1.0 equiv.) in a 2:1 mixture of ethanol/chloroform at 75°C for 12 hours. Purification was done according to the general procedure. The product **36** was obtained as an orange solid (90 mg, 72 % yield). Mp = 240 °C. ^{1}H NMR (300 MHz, Methanol-d_4 + 1 drop of D_2O) δ 8.84 (m, 4H or 4H+1H), 8.48 (dt, *J* = 8.1, 1.6 Hz, 1H), 8.10 (t, *J* = 7.0 Hz, 1H), 7.94 (d, *J* = 6.0 Hz, 2H), 7.87 (s, 1H), 7.08 (s, 1H), 6.73 (d, *J* = 8.5 Hz, 1H), 6.45 (d, *J* = 8.5 Hz, 1H), 5.38 (s, 2H). ^{13}C NMR (75 MHz, Methanol-d_4) δ 167.3, 157.0, 147.9, 147.2, 145.3, 144.5, 142.7, 141.3, 140.4, 136.5, 136.0, 131.8, 127.5, 124.7, 123.2, 111.8, 110.9, 107.8, 78.0. HRMS (ESI): calcd for $C_{21}H_{17}N_5O_3SNa$: [M +Na]$^+$: *m/z* 442.09443. Found: *m/z* 442.0938 (1 ppm). HPLC analysis, compound **24**: t_R = 9.7 min; purity: 99.6 %.

4-((*E*)-(((*Z*)-3-phenyl-4-(pyridin-4-yl)thiazol-2(3H)-ylidene) hydrazineylidene)methyl)benzene-1,2,3-triol,hydrobromide (25)

The reaction was performed with **22a** (184 mg, 0.61 mmol) and 2-bromo-1-pyridin-4-yl-ethanone (241 mg, 1.22 mmol) according to the general procedure. The product **25** was obtained as solid (155 mg, 52% yield), crystallised from ethanol. Mp = 256 °C. ^{1}H NMR (300 MHz, DMSO-d_6) δ 8.79 (d, *J* = 6.6 Hz, 2H), 8.33 (s, 1H), 7.69 (d, *J* = 6.6 Hz, 2H), 7.55 (s, 1H), 7.51 – 7.34 (m, 5H), 6.78 (d, *J* = 8.5 Hz, 1H), 6.38 (d, *J* = 8.5 Hz, 1H). ^{13}C NMR (75 MHz, DMSO-d_6) δ 166.1, 156.2, 149.0, 147.6, 145.5, 141.8, 136.3, 135.5, 132.5, 129.6(2C), 128.9, 128.3(C2), 124.5, 121.5,

112.1(2C), 111.2, 107.9. HRMS (ESI): calcd for $C_{21}H_{16}N_4O_3SNa$: $[M + Na]^+$: *m/z* 427.08408. Found: *m/z* 427.0843 (0 ppm). HPLC analysis, compound **25**: t_R = 17.8 min; purity: 99.0 %.

4-((*E*)-(((*Z*)-3,4-dibenzylthiazol-2(3H)-ylidene) hydrazineylidene)methyl)benzene-1,2,3-triol,hydrobromide (26)

The reaction was performed with **22b** (162 mg, 0.51 mmol) and 1-bromo-3-phenyl-propan-2-one (215 mg, 1.02 mmol) according to the general procedure. The product **26** was obtained as solid (145 mg, 55% yield), crystallised from acetone. Mp = 232 °C. ^{1}H NMR (400 MHz, DMSO-d_6): δ 8.36 (s, 1H), 7.39 – 7.23 (m, 6H), 7.22 – 7.15 (m, 4H), 6.79 (d, *J* = 8.5 Hz, 1H), 6.37 (d, *J* = 8.5 Hz, 1H), 6.12 (s, 1H), 5.14 (s, 2H), 3.80 (s, 2H). ^{13}C NMR (126 MHz, DMSO-d_6): δ 167.2, 153.4, 148.5, 147.4, 139.7, 136.1, 135.9, 132.5, 128.8, 128.7, 128.6, 127.3, 126.9, 126.1, 120.6, 111.3, 107.7, 99.5, 47.3, 33.1. HRMS (ESI): calcd for $C_{24}H_{21}N_3O_3SNa$: $[M + Na]^+$: *m/z* 454.12013. Found: *m/z* 454.1199 (0 ppm). HPLC analysis, compound **26**: t_R = 20.9 min; purity: 95.0 %.

4-((*E*)-(((*Z*)-3-benzyl-4-phenylthiazol-2(3H)-ylidene) hydrazineylidene)methyl)benzene-1,2,3-triol,hydrobromide (27)

The reaction was performed with **22b** (208 mg, 0.66 mmol) and 2-bromo-1-phenyl-ethanone (260 mg, 1.31 mmol) according to the general procedure. The product **27** was obtained as solid (170 mg, 51% yield), crystallised from acetone. Mp = 229 °C. ^{1}H NMR (300 MHz, DMSO-d_6) δ 8.41(s, 1H), 7.46-7.33 (m, 5H), 7.29-7.21 (m, 3H), 7.00 (d, 2d, *J* = 8.2 Hz), 6.82 (d, 1H, *J* = 8.6 Hz), 6.64 (s, 1H), 6.39 (d, 1H, *J* = 8.5 Hz), 5.10 (s, 2H). ^{1}H NMR (300 MHz, Methanol-d_4): δ 8.56 (s, 1H), 7.57 – 7.48 (m, 1H), 7.47 – 7.41 (m, 3H), 7.39 – 7.29 (m, 6H), 7.06 (d, *J* = 8.7 Hz, 1H), 7.03 (d, *J* = 1.1 Hz, 1H), 7.03 – 6.97 (m, 2H), 6.48 (d, *J* = 8.6 Hz, 1H), 5.31 (s, 2H). ^{13}C NMR (75 MHz, Methanol-d_4): δ 168.0, 152.3, 150.0, 147.6, 143.1, 133.6, 132.6, 130.2, 129.4, 128.8, 128.6, 128.4, 127.9, 125.7, 120.3, 110.8, 107.9, 106.0, 50.1, 48.4, 48.2, 47.9, 47.6, 47.3, 47.0, 46.7. HRMS (ESI): calcd for $C_{23}H_{19}N_3O_3SNa$: $[M + Na]^+$: *m/z* 440.10448. Found: *m/z* 440.1048 (0 ppm). HPLC analysis, compound **27**: t_R = 20.5 min; purity: 99.4 %.

4-((*E*)-(((*Z*)-3-benzyl-4-(4-chlorobenzyl)thiazol-2(3H)-ylidene) hydrazineylidene)methyl)benzene-1,2,3-triol,hydrobromide (28)

The reaction was performed with **22b** (205 mg, 0.64 mmol) and 1-bromo-3-(4-chlorophenyl)-propan-2-one (288 mg, 1.29 mmol) according to the general procedure. The product **28** was obtained as solid (276 mg, 81% yield), crystallised from acetone. Mp = 228 °C. ^{1}H NMR (300 MHz, DMSO-d_6) δ 8.39 (s, 1H), 7.38 – 7.26 (m, 5H), 7.26 – 7.19 (m, 2H), 7.17 – 7.12 (m, 2H), 6.81 (d, *J* = 8.5 Hz, 1H), 6.38 (d, *J* = 8.5 Hz, 1H), 6,19 (s, 1H), 5.16 (s, 2H), 3.83 (s, 2H). ^{13}C NMR (75 MHz, DMSO-d_6) δ 167.8, 153.5, 149.1, 147.9, 140.1, 136.2, 135.4, 133.0, 132.1, 131.1, 129.2, 129.0, 127.8, 126.6, 120.7, 111.8, 108.3, 101.0, 48.1, 32.9. HRMS (ESI): calcd for $C_{24}H_{20}{}^{35}ClN_3O_3S$: $[M + H]^+$: *m/z* 466.0992. Found: *m/z* 466.0992 (0 ppm). HPLC analysis, compound **28**: t_R = 16.4 min; purity: 98.5 %.

4-((*E*)-(((*Z*)-3-(4-chlorophenyl)-4-phenylthiazol-2(3H)-ylidene) hydrazineylidene)methyl)benzene-1,2,3-triol,hydrobromide (29)

The reaction was performed with **22d** (234 mg, 0.66 mmol) and 2-bromo-1-phenyl-ethanone (264 mg, 1.33 mmol) according to the general procedure. The product **29** was obtained as solid (198 mg, 55% yield), crystallised from acetone. Mp = 228 °C. ^{1}H NMR (300 MHz, DMSO-d_6): δ 8.34 (s, 1H), 7.45-7.39 (m, 3H), 7.36-7.31 (m, 4H), 7.01 (d, 1H, *J* = 8.4 Hz), 6.78 (d, 1H, *J* = 8.5 Hz), 6.54 (s, 1H), 6.38 (d, 1H, *J* = 8.4 Hz, 5.03 (s, 2H). ^{1}H NMR (300 MHz, Methanol-d_4 + 1 drop of D_2O): δ 8.58 (s, 1H), 7.53 (d, *J* = 7.3 Hz, 1H), 7.46 (t, *J* = 7.5 Hz, 2H), 7.35 (d, *J* = 7.7 Hz, 4H), 7.06 (d, *J* = 8.7 Hz, 1H), 7.01 (s, 2H), 6.99 (s, 1H), 6.49 (d, *J* = 8.6 Hz, 1H), 5.28 (s, 2H). ^{13}C NMR (75 MHz, Methanol-d_4 + 1 drop of D_2O): δ 167.8, 152.6, 150.2, 147.6, 142.9, 133.9, 132.7, 132.2, 130.4, 129.6, 128.8(2C), 128.7(2C), 128.2, 127.6 (2C), 120.8, 110.6, 108.1, 106.7, 49.8. HRMS (ESI): calcd for $C_{23}H_{18}ClN_3O_3SNa$: $[M + Na]^+$: *m/z* 474.06551. Found: *m/z* 474.0656 (0 ppm). HPLC analysis, compound **29**: t_R = 16.3 min; purity: 99.1 %.

4-((*E*)-(((*Z*)-3-(4-ethylbenzyl)-4-phenylthiazol-2(3H)-ylidene) hydrazineylidene)methyl)benzene-1,2,3-triol, hydrobromide (30)

The reaction was performed with **22e** (175 mg, 0.51 mmol) and 2-bromo-1-phenyl-ethanone (200 mg, 1.01 mmol) according to the general procedure. The product **30** was obtained as solid (135 mg, 50% yield), crystallised from acetone. Mp = 234 °C. ^{1}H NMR (300 MHz, DMSO-d_6) δ 8.36 (s, 1H), 7.48-7.40 (m, 3H), 7.38-7.36 (m, 2H), 7.09 (d, 2H, *J* = 8.1 Hz), 6.80-6.77 (m, 1H), 6.56-6.53 (m, 1H), 6.38 (d, 1H, *J* = 8.4 Hz), 5.03 (s, 2H), 2.52 (q, 2H, *J* = 7.6 Hz), 1.12 (s, 3H, *J* = 7.4 Hz). ^{1}H NMR (500 MHz, Methanol-d_4 + 1 drop of D_2O) δ 8.50 (s, 1H), 7.40 (m, 4H), 7.38 – 7.34 (m, 1H), 7.32 – 7.24 (m, 4H), 7.20 (s, 1H), 7.02 (d, *J* = 8.8 Hz, 1H), 6.48 (d, *J* = 8.8 Hz, 1H), 2.73 (q, *J* = 7.7 Hz, 2H), 1.27 (t, *J* = 7.7 Hz, 3H). ^{13}C NMR (126 MHz, Methanol-d_4 + 1 drop of D_2O): δ 169.8, 154.1, 151.4, 149.3, 148.8, 144.7, 134.0, 131.1(2C), 131.0, 130.8(2C), 129.7, 129.5(2C), 129.3(2C), 121.8, 112.1, 109.4, 107.8, 29.5, 15.7. HRMS (ESI): calcd for $C_{25}H_{23}N_3O_3SNa$: $[M + Na]^+$: *m/z* 468.13578. Found: *m/z* 468.1356 (0 ppm). HPLC analysis, compound **30**: t_R = 21.6 min; purity: 98.2 %.

4-((*E*)-(((*Z*)-3-(4-ethylphenyl)-4-phenylthiazol-2(3H)-ylidene) hydrazineylidene)methyl)benzene-1,2,3-triol, hydrobromide (31)

The reaction was performed with **22c** (203 mg, 0.61 mmol) and 2-Bromo-1-phenyl-ethanone (242 mg, 1.22 mmol) according to the general procedure. The product **31** was obtained as solid (177 mg, 57% yield), crystallised from ethanol. Mp = 230 °C. ^{1}H NMR (500 MHz, Methanol-d_4): δ 8.50 (d, *J* = 2.7 Hz, 1H), 7.40 (d, *J* = 2.6 Hz, 4H), 7.36 (dd, *J* = 11.6, 5.4 Hz, 1H), 7.33 – 7.26 (m, 4H), 7.19 (s, 1H), 7.02 (d, *J* = 8.8 Hz, 1H), 6.46 (d, *J* = 8.8 Hz, 1H), 2.73 (qd, *J* = 7.3, 2.1 Hz, 2H), 1.27 (t, *J* = 7.3, 3H). ^{13}C NMR (126 MHz, Methanol-d_4) δ 167.7, 152.0, 149.3, 147.2, 146.8, 142.6, 131.9, 129.0 (2C), 128.9, 128.7(2C), 127.6(2C), 127.4, 127.2(2C), 119.7, 110.0, 107.3, 105.7, 27.4, 13.6. HRMS (ESI): calcd for $C_{24}H_{21}N_3O_3SNa$: $[M + Na]^+$: *m/z* 454.12013. Found: *m/z* 454.1201 (0 ppm). HPLC analysis, compound **31**: t_R = 20.8 min; purity: 96.6 %.

4-((*E*)-(((*Z*)-4-phenyl-3-(pyridin-3-ylmethyl)thiazol-2(3H)-ylidene)hydrazineylidene)methyl)benzene-1,2,3-triol, hydrobromide (32)

The reaction was performed with **22g** (182 mg, 0.57 mmol) and 2-bromo-1-phenyl-ethanone (226 mg, 1.14 mmol) according to the general procedure. The product **32** was obtained as solid (150 mg, 53% yield), crystallised from ethanol. Mp = 258 °C. ^{1}H NMR (300 MHz, DMSO-d_6): δ 8.81 (d, 1H, *J* = 5.2 Hz), 8.68 (d, 1H, *J* = 1.5 Hz), 8.31 (s, 1H), 8.23 (d, 1H, *J* = 8.3Hz), 7.98 (dd, 1H, *J* = 8.1, 5.7 Hz), 7.49-7.44 (m, 3H), 7.41-7.37 (m, 2H), 6.75 (d, 1H, *J* = 8.6 Hz), 6.56 (s, 1H), 6.38 (d, 1H, *J* = 8.4 Hz), 5.16 (s, 2H). ^{1}H NMR (300 MHz, Methanol-d_4 + 1 drop of D_2O): δ 8.80 (d, *J* = 5.7 Hz, 1H), 8.68 (d, *J* = 2.0 Hz, 1H), 8.44 (s, 1H), 8.39 (d, *J* = 8.2 Hz, 1H), 8.07 (dd, *J* = 8.2, 5.8 Hz, 1H), 7.46 – 7.39 (m, 2H), 6.85 (d, *J* = 8.6 Hz, 1H), 6.60 (s, 1H), 6.47 (d, *J* = 8.5 Hz, 1H), 5.39 (s, 2H). ^{13}C NMR (75 MHz, Methanol-d_4 + 1 drop of D_2O): 168.8, 156.3, 151.4, 149.3, 146.7, 142.2, 141.9, 138.2, 134.0, 131.6, 130.8 (2C), 130.5 (2C), 130.3, 129.6, 128.8 123.6, 112.0, 109.3, 103.9, 47.7. HRMS (ESI): calcd for $C_{22}H_{18}N_4O_3SNa$: [M + Na]$^+$: *m/z* 441.09973. Found: *m/z* 441.0999 (0 ppm). HPLC analysis, compound **32**: t_R = 12.1 min; purity: 96.0 %.

4-((*E*)-(((*Z*)-4-phenyl-3-(pyridin-3-yl)thiazol-2(3H)-ylidene) hydrazineylidene)methyl)benzene-1,2,3-triol, hydrobromide (33)

The reaction was performed with **22f** (225 mg, 0.74 mmol) and 2-bromo-1-phenyl-ethanone (293 mg, 1.48 mmol) according to the general procedure. The product **33** was obtained as solid (191 mg, 53% yield), crystallised from acetone. Mp = 252 °C. ^{1}H NMR (500 MHz, Methanol-d_4): δ 9.09 (d, *J* = 2.3 Hz, 1H), 8.81 (d, *J* = 5.6 Hz, 1H), 8.45 (ddd, *J* = 8.5, 2.3, 1.3 Hz, 1H), 8.35 (s, 1H), 8.02 (dd, *J* = 8.5, 5.6 Hz, 1H), 7.44 – 7.35 (m, 3H), 7.33 – 7.27 (m, 2H), 6.82 (d, *J* = 8.6 Hz, 1H), 6.80 (s, 1H), 6.47 (d, *J* = 8.6 Hz, 1H). ^{13}C NMR (126 MHz, Methanol-d_4): δ 167.4, 157.7, 150.2, 148.6, 145.2, 143.9, 142.8, 140.1, 137.2, 133.3, 130.3, 129.9, 129.8, 129.6, 127.8, 123.0, 111.9, 108.5, 104.4. HRMS (ESI): calcd for $C_{21}H_{16}N_4O_3SNa$: [M + Na]$^+$: *m/z* 427.08408. Found: *m/z* 427.0841 (0 ppm). HPLC analysis, compound **33**: t_R = 11.5 min; purity : 96.9 %.

4-((*E*)-(((*Z*)-3-benzyl-4-(pyridin-3-yl)thiazol-2(3H)-ylidene)hydrazineylidene)methyl) benzene-1,2,3-triol (34)

The reaction was performed with **22b** (158 mg, 0.5 mmol) and 3-(bromoacetyl)pyridine hydrobromide (281 mg, 1.0 mmol) according to the general procedure. The product **34** was obtained as orange solid (189 mg, 76% yield). Mp = 218 °C. ^{1}H NMR (300 MHz, Methanol-d_4 + 1 drop of D_2O): δ 8.84 (d, *J* = 5.8 Hz, 1H), 8.71 (s, 1H), 8.41 (s, 1H), 8.37 (dt, *J* = 8.2, 1.7 Hz, 1H), 7.99 (dd, *J* = 8.1, 5.7 Hz, 1H), 7.30 (m, 3H), 7.03 (dd, *J* = 7.4, 2.0 Hz, 2H), 6.88(s, 1H), 6.83 (d, *J* = 8.6 Hz, 1H), 6.48 (d, *J* = 8.5 Hz, 1H), 5.24 (s, 2H). ^{13}C NMR (75 MHz, Methanol-d_4 + 1 drop of D_2O): δ 167.8, 155.1, 148.7, 147.4, 144.9, 143.2, 142.5, 135.3, 134.8, 132.3, 129.7, 128.8, 127.8, 126.8, 126.2, 122.0, 111.5, 107.6, 106.6, 49.3. HRMS (ESI): calcd for $C_{22}H_{18}N_4O_3SNa$: [M + Na]$^+$: *m/z* 441.09973. Found: *m/z* 441.0994 (0 ppm). HPLC analysis, compound **34**: t_R = 12.2 min; purity: 98.7 %.

4-((*E*)-(((*Z*)-3-benzyl-4-(pyridin-4-yl)thiazol-2(3H)-ylidene)hydrazineylidene)methyl) benzene-1,2,3-triol (35)

The reaction was performed with **22b** (158 mg, 0.5 mmol) and 4-(bromoacetyl)pyridine hydrobromide (281 mg, 1.0 mmol) according to the general procedure. The product 35 was obtained as orange solid (184 mg, 74% yield). Mp = 186 °C. ^{1}H NMR (300 MHz, DMSO-d_6): δ 11.01 (s, 1H), 8.89 (d, *J* = 6.1 Hz, 2H), 8.41 (s, 1H), 7.92 (d, *J* = 6.4 Hz, 2H), 7.26 (m, 3H), 7.15 (s, 1H), 7.09 – 7.02 (m, 2H), 6.81 (d, *J* = 8.5 Hz, 1H), 6.40 (d, *J* = 8.5 Hz, 1H), 5.21 (s, 2H). ^{13}C NMR (75 MHz, DMSO-d_6): δ 166.8, 156.1, 149.2, 148.0, 144.6, 137.2, 136.6, 133.0, 129.2, 128.0, 127.0, 125.1, 122.1, 111.8, 108.3, 49.3. HRMS (ESI): calcd for $C_{22}H_{18}N_5O_3SNa$: [M + Na]$^+$: *m/z* 441.09973 Found: *m/z* 441.0991 (0 ppm). HPLC analysis, compound **35**: t_R = 12.3 min; purity: 97.0 %.

MIM1 (compound 2) Studies

General comments on NMR experiments for MIM1 and analogues

MIM1 (**2**) is a hydrochloride and not a neutral compound as previously reported. Extensive studies, under different conditions, have been required in order to obtain complete 1D and 2D NMR data for these molecules, as described here. For instance, one proton of the cyclohexyl moiety was hidden by the residual peaks of DMSO-d_6 and this peak has been well established by 2D correlation COSY experiment at 343 K. Secondly, direct ^{13}C NMR experiment could not give the full set of ^{13}C peaks. In DMSO-d_6, dynamic effects and slow relaxation processes appeared to be connected to the observed broad and large peaks in ^{13}C and ^{1}H spectra. Furthermore, in the case of ^{1}H spectrum such dynamic effects are responsible for the completely change of the spectrum when concentration increased by a factor 4 (25 mg/mL) but with a reversible issue upon dilution, this different limitation tends to limit direct ^{13}C NMR experiment and to be completed by 2D NMR ones. Then, to sort out such difficulties 2D correlation experiments at variable temperatures from 313 to 343 K have been tuned to release the dynamic effects observed, permit relaxation process to occur and then allow to have access to all carbon NMR peaks (HSQC, HMBC experiment at 343 K). Finally, ^{13}C experiment in DMSO-d_6 were run at 343 K and give the full set of data. In SI are presented one example of such effect seen on ^{1}H NMR spectra (Fig. 1) and relevant spectra. Nevertheless, after overpassing those difficulties compound **2** was characterised in DMSO-d_6. Then, we tested DMF-d_7 and MeOH-d_4 as two others deuterated solvents. Unfortunately, the first one presents equivalent dynamic effects like those observed with DMSO-d_6 and for the second one, compound **2** as hydrochloride was not soluble, even with drops of D_2O added, in opposition of the hydrobromides analogues.

Synthesis of MIM1: 4-((*E*)-(((*Z*)-3-cyclohexyl-4-methylthiazol-2(3H)-lidene)hydrazineylidene) methyl)benzene-1,2,3-triol, hydrochloride (2)

Compound **2** and intermediates were prepared according to the procedure described by Cohen and Walenski,[33] and yielded a colorless powder in 85 % yield. Mp = 200°C, (Litt: unknown). Microanalysis: Anal. Found: C, 53.16; H, 5.69; N 10.87; S, 8.35 Calcd for $C_{17}H_{22}N_3O_3ClS$: C, 53.19; H, 5.78; N, 10.95; S, 8.35. FT-

IR (Powder) ν_{max}/cm^{-1} 3138, 2927, 2856, 2816, 2758, 1625, 1568, 1516, 1336, 1265, 976, 809. ^{1}H NMR (500 MHz, 300K, DMSO-d_6) δ 8.42 (s, 1H), 6.80 (d, *J* = 8.5 Hz, 1H), 6.40 (d, *J* = 8.4 Hz, 1H), 6.11 (s, 1H), 4.12 (m, 1H), 2.23 (s, 3H), 1.90 – 1.80 (m, 3H), 1.78 – 1.70 (m, 2H), 1.66 (d, *J* = 13.0 Hz, 1H), 1.40 (qt, *J* = 13.0, 3.6 Hz, 2H), 1.30 – 1.17 (m, 1H). (one proton at 2.5 ppm is hidden by the residual DMSO solvent and observed by COSY correlation). ^{13}C NMR (126 MHz NUS sampling, DMSO at 343 K) δ 167.5, 153.2, 149.0, 148.0, 137.8, 133.2, 121.0, 112.3, 108.4, 98.4, 58.5, 29.2, 26.1, 25.2, 15.9. HRMS (ESI): calcd for $C_{17}H_{22}N_3O_3S$: [M + H]$^+$: *m/z* 348.13819, Found: *m/z* 348.1377 (0 ppm). HPLC analysis, compound **2**: t_R = 15.0 min; purity: 98.3 %. Noesy NMR experiment performed at 500 MHz in DMSO-d_6 shows spatial proximity between methyl and cyclohexyl groups, imine proton and H aromatics ones, methyl and ethylenic proton, and proton of cyclohexyl group hidden by residual DMSO and others protons of cyclohexyl group. 2D Cosy NMR experiment done at 500 MHz in DMSO-d_6 shows correlation between hidden proton by residual DMSO solvent peak and others from cyclohexyl group. 2D HSQC and HMBC NMR experiments at 343K completed carbons peaks not seen directly by ^{13}C NMR experiment neither at 273K or 343 K.

Synthesis and analyses of compound 11

In order to confirm the structure **2** for MIM1 and to determine its stereochemistry the 2,3,4-trimethoxy analogue (**11**) was synthesised with the same general procedure in place of 2,3,4-trihydroxy one.

(*Z*)-3-cyclohexyl-4-methyl-2-(((*E*)-2,3,4-trimethoxybenzylidene)hydrazineylidene)-2,3-dihydrothiazole, hydrochloride (11)

Compound **11** was prepared by the same general procedure as mentioned above, starting from trimethoxy benzaldehyde. It was obtained as a colorless powder in 88 % yield. Compound **11** was subjected also to ^{1}H and ^{13}C NMR analysis which confirmed previous results. In the same way as for MIM1 (**2**), NMR experiments show slow relaxations processes upon temperature variation (cf. SI, Fig. 1). Noesy experiment done at spectrum at 353 K proved spatial correlation between methyl and cyclohexyl groups without ambiguity, below this temperature a weak signal could be distinguished after rising the temperature.

Mp = 152°C. Microanalysis: Anal. Found: C, 55.70; H, 6.47; N 9.78; S, 7.35. Calcd for $C_{20}H_{28}N_3O_3ClS$. (¼ H_2O): C, 55.75; H, 6.50; N, 9.75; S, 7.43. IR (powder) ν_{max}/cm^{-1} 3311, 2935, 2859, 2500, 1589, 1570, 1498, 1440, 1410, 1295, 1100, 1082, 866, 809, 749. ^{1}H NMR (400 MHz, DMF-d_7 at 343K): δ 9.07 (s, 1H), 7.66 (d, *J* = 8.8 Hz, 1H), 6.97 (d, *J* = 8.8 Hz, 1H), 6.52 (s, 1H), 4.79 (s, 1H), 3.96 (s, 3H), 3.95 (s, 4H), 3.87 (s, 3H), 2.43 (s, 4H), 2.01 – 1.80 (m, 5H), 1.68 (d, *J* = 12.8 Hz, 3H), 1.44 – 1.21 (m, 1H). (one proton hidden by the methyl group). ^{1}H NMR (500 MHz, $CDCl_3$): δ 15.50 (s, 1H), 9.47 (s, 1H), 7.56 (d, *J* = 8.8 Hz, 1H), 6.71 (d, *J* = 8.8 Hz, 1H), 6.30 (s, 1H), 5.41 (s, 1H), 4.00 (s, 3H), 3.91 (s, 3H), 3.88 (s, 3H), 2.47 (s, 3H), 2.08 (s, 3H), 1.96 (s, 2H), 1.91 (s, 2H), 1.80 (d, *J* = 13.5 Hz, 1H), 1.28 (s, 2H). ^{13}C NMR (126 MHz NUS sampling, $CDCl_3$, 300 K) δ 169.2, 156.3, 154.1, 149.7, 142.2, 139.2, 122.2, 120.1, 107.7, 106.0, 62.1, 61.5, 60.9, 56.1, 31.1, 25.3, 25.0, 17.3. HRMS (ESI): calcd for $C_{20}H_{28}N_3O_3S$: [M + H]$^+$: *m/z* 390.18514. Found: *m/z* 390.1849 (1 ppm). HPLC analysis, compound **11**: t_R = 18.5 min; purity: 95.9 %.

Single crystal structures suitable for X-ray analysis were grown by slow diffusion layer/layer of pentane into a solution of compound **11** in chloroform at 20°C. The details of X-Ray structural analysis of **11** have been deposited at CDDC with the number 2006656.

Synthesis and analyses of compound 14a and 14b

Compounds **14a** and **14b** were synthesised with the same general procedure as mentioned in 7.1.3, starting respectively with 4-methoxybenzaldehyde and tolylaldehyde.

(4-Methoxy-benzylidene)-(4-phenyl-2-phenylimino-thiazol-3-yl)-amine (14a)

The product **14a** was obtained as white crystals (268 mg, 78% yield). Mp = 227°C. RMN ^{1}H (methanol-d4, 300 MHz): 8.29 (s, 1H), 7.74-7.71 (m, 2H), 7.59-7.55 (m, 3H), 7.54-7.49 (m, 2H), 7.30-7.23 (m, 5H), 7.05-7.00 (m, 3H), 3.86 (s, 3H). RMN ^{13}C (Methanol-d_4, 75 MHz): 170.9, 164.2, 153.5, 144.5, 135.4, 132.5, 131.8 (2C), 131.1, 130.9 (4C), 129.7, 129.6 (2C), 129.5 (2C), 126.6, 115.6 (2C), 108.7, 56.1. HRMS (ESI): calcd for $C_{23}H_{19}N_3OSNa$: [M + Na]$^+$: *m/z* 408.11465. Found: *m/z* 408.1167 (5 ppm).

Single crystal structures suitable for X-ray analysis were grown by slow evaporation of a solution of compound **14a** in acetone at 20°C. The details of X-Ray structural analysis of **14a** have been deposited at CDDC with the number 2006657.

(4-Methyl-benzylidene)-(4-phenyl-2-phenylimino-thiazol-3-yl)-amine (14b)

The product **14b** was obtained as yellow crystals (237 mg, 77% yield). Mp = 223 °C. RMN ^{1}H (Methanol-d_4, 300 MHz): 8.74 (s, 1H), 7.66 (dt, 2H, *J* = 8.3 Hz, *J* = 1.8 Hz), 7.59-7.54 (m, 3H), 7.53-7.49(m, 2H), 7.38-7.29 (m, 4H), 7.28 (s, 1H), 7.27-2.25 (m, 3H), 2.39 (3H). RMN ^{13}C (Methanol-d_4, 75 MHz): 171.1, 153.9, 144.6, 143.8, 135.0, 132.6, 131.8 (2C), 131.4, 131.1, 130.9 (2C), 130.8 (2C), 129.6 (3C), 129.5, 129.1, 109.0, 21.7. HRMS (ESI): calcd for $C_{23}H_{20}N_3S$: [M + H]$^+$: *m/z* 370.13779. Found: *m/z* 370.1375 (1 ppm). Single crystal structures suitable for X-ray analysis were grown by slow evaporation of a solution of compound **14b** in acetone at 20°C. The details of X-Ray structural analysis of **14b** have been deposited at CDDC with the number 2006655.

Flexible docking

Compounds were docked with a flexible docking protocol in order to consider both ligand and protein flexibility, using ChiFlex, LibDock and CDocker, as implemented in Discovery Studio v17.1 (Biovia, Dassault Systemes, San Diego, CA). The coordinates of crystallised proteins were PDB:3KJ0[73] and PDB:3SPF,[74] for Mcl-1 and Bcl-x_L respectively. The site sphere was set to 18 Å around co-crystallised ligands. 100 hot spots were considered for docking, and simulated annealing was used to refine the complexes, with 2000 heating steps at 700 K followed by 5000 cooling steps at 300 K. Protein conformers

were obtained by 38° minimum side chain angle rotations. 73 protein conformers were generated with Mcl-1 and 55 for Bcl-x_L.

MCSS

Multiple Copy Simultaneous Search (MCSS)[75] was carried out on a 18 Å sphere encompassing co-crystallised ligand. 8000 fragment replicas were initially placed in the receptor cavities, and poses were optimised by 10,000 steps of Powel minimization, following 8000 steps of steepest descent, using CHARMm force-field. Binding free energy was calculated using a molecular mechanics Poisson-Boltzmann with a non-polar surface area implicit solvent model (MM-PBSA), as described with MM-GBSA.[76]

Molecular dynamics

The modelled complexes (Mcl-1/**35** or Bcl-x_L/**35**) were inserted in a water box of 76 x 58 x 61 Å consisting of 8756 water molecules and 2 chloride ions to equilibrate the system, 62 x 57 x 57 Å consisting of 6667 water molecules and 6 sodium ions, respectively for Mcl-1 and Bcl-x_L, in explicit periodic boundary conditions. Optimization of the solvent molecules was performed by 6000 steps of steepest descent energy minimization, keeping the inhibitor/protein complex frozen. Then the ensemble was again subjected to energy minimization (5000 steps of steepest descent then adopted Newton Raphson), heating (200 ps from 50 to 300 K), and equilibration (200 ps at 300 K). The production (3 independent runs of 100 ns) was performed using NAMD v2.9 in NPT conditions, with a timestep of 2 fs at 300 K. The non-bond pairlist distance was set to 14 Å, the cut off to 12 Å and a switching distance of 10 Å. A multiple time stepping integration was used, with a mollified impulse method (MOLLY). A Langevin dynamics was used for the temperature control, and a Langevin piston for the pressure control. All hydrogen-atoms bonds were kept rigid (SHAKE), and the SETTLE algorithm was used for water molecules.

FPA assay

Carboxy-fluorescein labelled peptide (5-FAM-EDIIRNIARHLAQVGDSMDR-NH_2) and Bim-WT peptide (H-Ahx-DMRPEIWIAQELRRIGDEFNAYYAR-OH) were purchased from GENEPEP and used without further purification. Mcl-1 (172-327) was produced in collaboration with Biomolecules laboratory of Pierre and Marie Curie University.[77] FPA measurements were carried out in 96-well, black, flat-bottom plates (Greiner Bio-One) using the Bioteck microplate reader Synergy 2. All assays were conducted in assay buffer containing 20 mM Na_2HPO_4 (pH 7.4), 50 mM NaCl, 2 µM EDTA, 0.05% Pluronic F-68.[78] For IC_{50} determination, compounds were diluted in DMSO in a 8-point, serial dilution scheme, added to assay plates and were incubated with 100 nM Mcl-1 for two hours. Then, to measure inhibition of Mcl-1/FAM-Bid interaction, 15 nM 5-FAM-Bid peptide was added and plates were incubated for two hours at room temperature. For each experiment, a negative control containing Mcl-1 and 5-FAM-Bid peptide (equivalent to 0% inhibition), and a positive control containing Mcl-1, 5-FAM-Bid peptide, and 10 µM Bim-WT peptide (equivalent to 100% inhibition), were included on each assay plate. Each point was duplicated and each experiment was performed in two biological replicates. The change in polarization was measured and used to calculate an IC_{50} (inhibitor concentration at which 50% of bound peptide is displaced), by fitting the inhibition data using GraphPad Prism 6 software to a sigmoïdal, 4PL, X is log(concentration). This was converted into a binding dissociation constant (Ki) according to the formula described by Nikolovska-Coleska *et al.*[68]

Cell culture and treatment

IGROV1-R10 cell line was established as described previously[79] from the IGROV1 cell line, itself kindly provided by Dr. Jean Bénard (Institut Gustave Roussy, Paris, France). They were grown in RPMI1640 (Gibco) medium supplemented with 2 mM Glutamax™, 25 mM HEPES (4-(2-hydroxyethyl)-1-piperazineethanesulfonic acid), 10% decomplemented FBS (Fetal Bovine Serum) (Gibco) and 33 mM sodium bicarbonate (Gibco) and were maintained in a 5% CO_2 humidified atmosphere at 37 °C. Ovarian cancer cell lines were certified mycoplasma-free thank to a MycoAlert test. Cells were seeded in 25 cm2 flasks 24 hours before their treatment and exposed to MIM1 or analogue molecules as single agents or in combination with ABT-737 or S63845 for 24 hours at the indicated concentrations.

Nuclei staining by DAPI

After treatment, both detached and adherent cells were pooled after trypsinization, applied to a polylysine-coated glass slide by cytocentrifugation and fixed with a solution of ethanol/chloroform/acetic acid (6:3:1). The preparations were then incubated for 15min at room temperature with 1µg/ml DAPI solution (Boehringer Mannheim-Roche, Mannheim, Germany), washed in distilled water, mounted under a coverslip in Mowiol (Calbiochem) and analysed under a fluorescence microscope (BX51, Olympus, Rungis, France).

On each image a deep-learning-based method of 2D nucleus detection was applied [Uwe Schmidt, Martin Weigert, Coleman Broaddus, and Gene Myers. Cell Detection with Star-convex Polygons. International Conference on Medical Image Computing and Computer-Assisted Intervention [MICCAI, Granada, Spain, September 2018] with a python program. A size filter was used to class intact nuclei and fragmented nuclei. Then, a closing morphological operator was applied to regroup the clusters of small fragments. Each cluster was counted as one fragmented nuclei.

DNA content analysis by flow cytometry

Adherent and floating cells were pooled, washed with 1X PBS and fixed with ethanol 70°. Before flow cytometry analysis, cells were centrifuged at 2000 rpm for 5 min and incubated for 30 min at 37°C in PBS to allow the release of low-molecular weight DNA (characteristic of apoptotic cells). Cell pellets were

stained with propidium iodide (PI) using the DNA Prep Coulter Reagent Kit (Beckman-Coulter, Villepinte France). Samples were thereafter analysed using a Gallios flow cytometer (Beckman Coulter) and cell cycle distribution was determined using Kaluza acquisition software (Beckman Coulter).

Western blot analyses

Cells were rinsed with ice-cold PBS, suspended in a lysis buffer [RIPA : NaCl 150mM, Tris (pH 8) 50mM, Triton X100 1%, PMSF 4mM, EDTA 5mM, NaF 10mM, NaPPi 10mM, Na3OV4 1mM, aprotinin 0.5µL/mL and 4.6 mL ultra-pure water] and incubated on ice for 30min. Lysates were collected after centrifugation (13200g, 10 min, 4°C) and protein concentrations were determined using the Bradford assay (Bio-Rad, Hercules, USA). 25µg of protein were separated by SDS–PAGE on a 4-15% gradient polyacrylamide gel (Invitrogen, Cergy-Pontoise, France) and transferred to Hybond-PVDF membranes (Amersham, Orsay, France). After blocking non-specific binding sites for 1 hour at RT by 5% (w/v) non-fat dry milk in TBS with 0.1% (v/v) Tween20 (T-TBS), the membranes were incubated overnight at 4°C with the following rabbit monoclonal antibody: PARP, caspase-3 (Cell Signaling Technology, Ozyme, Saint-Quentin-en-Yvelines, France) or mouse monoclonal antibody: actin (EMD, Millipore, France). Membranes were then washed with T-TBS and incubated for 1 hour with the appropriate horseradish peroxidase-conjugated anti-rabbit (Cell Signaling Technology, France) or anti-mouse (Amersham, Orsay, France) secondary antibodies. Revelation was done using a luminescent Image Analyzer (GE Healthcare, Orsay, France). Quantification was performed with the ImageQuantTL software (version 7.0).

Conflicts of interest

There are no conflicts to declare.

Acknowledgements

We thank CNRS and University of Rennes 1 for their support. Financial support by the “Ligue contre le Cancer, Conseil Interrégional Grand Ouest” and “Ligue Contre le Cancer, Conseil Interrégional de Normandie et Comité du Calvados” is gratefully acknowledged. This work was also supported by the “Conseil Régional de Basse Normandie” and European Union (The ONCOTHERA European project “Normandy Network for innovative therapeutics in oncology” which is co-funded by the Normandy County Council, the European Union within the framework of the Operational Programme ERDF/ESF 2014-2020), by the French State (CPER Innovons 2), the University of Caen Normandie and Inserm. This research has been supported in Lebanon by the Research Grant program at the Lebanese University. The authors would like to acknowledge the National Council for Scientific Research of Lebanon (CNRS-L)/Agence Universitaire de la Francophonie (AUF)/and the Lebanese University (UL) for granting a doctoral fellowship to A. S. We are very grateful to the Centre Régional de Mesures Physiques de l’Ouest, Rennes (CRMPO) team for the HRMS analyses plus various NMR studies and for very fruitful discussions. We gratefully acknowledge Mrs Aurélie Sauvager (Pr J. Boustie’s group, Rennes) for the HPLC analyses. We thank European FEDER founds for acquisition of D8Venture X-ray diffractometer used for crystal structure determination. SH and HP were recipient of a doctoral fellowship from the “Ministère de l’Enseignement Supérieur, de la Recherche et de l’Innovation” granted by Normandy Doctoral School 497 “EDN Bise“. We acknowledge Maryline Guillamin (Flow cytometry accommodation, SF 4206 ICORE, University of Caen Normandie), for her helpful technical support and Pr Khaled Meflah and Pr Marc André Mahé, successive heads of the Comprehensive Cancer Center François Baclesse, for their constant support.

References

1. C. Fitzmaurice, C. Allen, R. M. Barber, L. Barregard, Z. A. Bhutta, H. Brenner, D. J. Dicker, O. Chimed-Orchir, R. Dandona, L. Dandona, T. Fleming, M. H. Forouzanfar, J. Hancock, R. J. Hay, R. Hunter-Merrill, C. Huynh, H. D. Hosgood, C. O. Johnson, J. B. Jonas, J. Khubchandani, G. A. Kumar, M. Kutz, Q. Lan, H. J. Larson, X. Liang, S. S. Lim, A. D. Lopez, M. F. MacIntyre, L. Marczak, N. Marquez, A. H. Mokdad, C. Pinho, F. Pourmalek, J. A. Salomon, J. R. Sanabria, L. Sandar, B. Sartorius, S. M. Schwartz, K. A. Shackelford, K. Shibuya, J. Stanaway, C. Steiner, J. Sun, K. Takahashi, S. E. Vollset, T. Vos, J. A. Wagner, H. Wang, R. Westerman, H. Zeeb, L. Zoeckler, F. Abd-Allah, M. B. Ahmed, S. Alabed, N. K. Alam, S. F. Aldhahri, G. Alem, M. A. Alemayohu, R. Ali, R. Al-Raddadi, A. Amare, Y. Amoako, A. Artaman, H. Asayesh, N. Atnafu, A. Awasthi, H. B. Saleem, A. Barac, N. Bedi, I. Bensenor, A. Berhane, E. Bernabe, B. Betsu, A. Binagwaho, D. Boneya, I. Campos-Nonato, C. Castaneda-Orjuela, F. Catala-Lopez, P. Chiang, C. Chibueze, A. Chitheer, J. Y. Choi, B. Cowie, S. Damtew, J. das Neves, S. Dey, S. Dharmaratne, P. Dhillon, E. Ding, T. Driscoll, D. Ekwueme, A. Y. Endries, M. Farvid, F. Farzadfar, J. Fernandes, F. Fischer, G. H. TT, A. Gebru, S. Gopalani, A. Hailu, M. Horino, N. Horita, A. Husseini, I. Huybrechts, M. Inoue, F. Islami, M. Jakovljevic, S. James, M. Javanbakht, S. H. Jee, A. Kasaeian, M. S. Kedir, Y. S. Khader, Y. H. Khang, D. Kim, J. Leigh, S. Linn, R. Lunevicius, H. M. A. El Razek, R. Malekzadeh,

D. C. Malta, W. Marcenes, D. Markos, Y. A. Melaku, K. G. Meles, W. Mendoza, D. T. Mengiste, T. J. Meretoja, T. R. Miller, K. A. Mohammad, A. Mohammadi, S. Mohammed, M. Moradi-Lakeh, G. Nagel, D. Nand, Q. Le Nguyen, S. Nolte, F. A. Ogbo, K. E. Oladimeji, E. Oren, M. Pa, E. K. Park, D. M. Pereira, D. Plass, M. Qorbani, A. Radfar, A. Rafay, M. Rahman, S. M. Rana, K. Soreide, M. Satpathy, M. Sawhney, S. G. Sepanlou, M. A. Shaikh, J. She, I. Shiue, H. R. Shore, M. G. Shrime, S. So, S. Soneji, V. Stathopoulou, K. Stroumpoulis, M. B. Sufiyan, B. L. Sykes, R. Tabares-Seisdedos, F. Tadese, B. A. Tedla, G. A. Tessema, J. S. Thakur, B. X. Tran, K. N. Ukwaja, B. S. C. Uzochukwu, V. V. Vlassov, E. Weiderpass, M. Wubshet Terefe, H. G. Yebyo, H. H. Yimam, N. Yonemoto, M. Z. Younis, C. Yu, Z. Zaidi, M. E. S. Zaki, Z. M. Zenebe, C. J. L. Murray and M. Naghavi, *JAMA Oncol*, 2017, **3**, 524-548.

2. J. M. Adams and S. Cory, *Cell Death Differ*, 2018, **25**, 27-36.
3. A. R. Delbridge and A. Strasser, *Cell Death Differ*, 2015, **22**, 1071-1080.
4. H. C. Zheng, *Oncotarget*, 2017, **8**, 59950-59964.
5. K. Li, *Bioorg Med Chem Lett*, 2021, **32**, 127717.
6. A. Negi and P. V. Murphy, *Eur J Med Chem*, 2021, **210**, 113038.
7. K. E. Tagscherer, A. Fassl, B. Campos, M. Farhadi, A. Kraemer, B. C. Bock, S. Macher-Goeppinger, B. Radlwimmer, O. D. Wiestler, C. Herold-Mende and W. Roth, *Oncogene*, 2008, **27**, 6646-6656.
8. S. K. Tahir, X. Yang, M. G. Anderson, S. E. Morgan-Lappe, A. V. Sarthy, J. Chen, R. B. Warner, S. C. Ng, S. W. Fesik, S. W. Elmore, S. H. Rosenberg and C. Tse, *Cancer Res*, 2007, **67**, 1176-1183.
9. E. Wesarg, S. Hoffarth, R. Wiewrodt, M. Kroll, S. Biesterfeld, C. Huber and M. Schuler, *Int J Cancer*, 2007, **121**, 2387-2394.
10. T. Oltersdorf, S. W. Elmore, A. R. Shoemaker, R. C. Armstrong, D. J. Augeri, B. A. Belli, M. Bruncko, T. L. Deckwerth, J. Dinges, P. J. Hajduk, M. K. Joseph, S. Kitada, S. J. Korsmeyer, A. R. Kunzer, A. Letai, C. Li, M. J. Mitten, D. G. Nettesheim, S. Ng, P. M. Nimmer, J. M. O'Connor, A. Oleksijew, A. M. Petros, J. C. Reed, W. Shen, S. K. Tahir, C. B. Thompson, K. J. Tomaselli, B. Wang, M. D. Wendt, H. Zhang, S. W. Fesik and S. H. Rosenberg, *Nature*, 2005, **435**, 677-681.
11. D. Chauhan, M. Velankar, M. Brahmandam, T. Hideshima, K. Podar, P. Richardson, R. Schlossman, I. Ghobrial, N. Raje, N. Munshi and K. C. Anderson, *Oncogene*, 2007, **26**, 2374-2380.
12. K. Simonin, M. N'Diaye, S. Lheureux, C. Loussouarn, S. Dutoit, M. Briand, F. Giffard, E. Brotin, C. Blanc-Fournier and L. Poulain, *Apoptosis*, 2013, **18**, 492-508.
13. K. Simonin, E. Brotin, S. Dufort, S. Dutoit, D. Goux, M. N'Diaye, C. Denoyelle, P. Gauduchon and L. Poulain, *Mol Cancer Ther*, 2009, **8**, 3162-3170.
14. S. Lheureux, M. N'Diaye, C. Blanc-Fournier, A. E. Dugue, B. Clarisse, S. Dutoit, F. Giffard, E. Abeilard, M. Briand, A. Labiche, J. M. Grellard, H. Crouet, S. Martin, F. Joly and L. Poulain, *Int J Cancer*, 2015, **136**, E340-350.
15. J. Chen, S. Jin, V. Abraham, X. Huang, B. Liu, M. J. Mitten, P. Nimmer, X. Lin, M. Smith, Y. Shen, A. R. Shoemaker, S. K. Tahir, H. Zhang, S. L. Ackler, S. H. Rosenberg, H. Maecker, D. Sampath, J. D. Leverson, C. Tse and S. W. Elmore, *Mol Cancer Ther*, 2011, **10**, 2340-2349.
16. W. H. Wilson, O. A. O'Connor, M. S. Czuczman, A. S. LaCasce, J. F. Gerecitano, J. P. Leonard, A. Tulpule, K. Dunleavy, H. Xiong, Y. L. Chiu, Y. Cui, T. Busman, S. W. Elmore, S. H. Rosenberg, A. P. Krivoshik, S. H. Enschede and R. A. Humerickhouse, *Lancet Oncol*, 2010, **11**, 1149-1159.
17. A. W. Roberts, M. S. Davids, J. M. Pagel, B. S. Kahl, S. D. Puvvada, J. F. Gerecitano, T. J. Kipps, M. A. Anderson, J. R. Brown, L. Gressick, S. Wong, M. Dunbar, M. Zhu, M. B. Desai, E. Cerri, S. Heitner Enschede, R. A. Humerickhouse, W. G. Wierda and J. F. Seymour, *N Engl J Med*, 2016, **374**, 311-322.
18. S. Fletcher, *Expert Opin Ther Pat*, 2019, **29**, 909-919.
19. L. M. Juarez-Salcedo, V. Desai and S. Dalia, *Drugs Context*, 2019, **8**, 212574.
20. E. F. Lee, T. J. Harris, S. Tran, M. Evangelista, S. Arulananda, T. John, C. Ramnac, C. Hobbs, H. Zhu, G. Gunasingh, D. Segal, A. Behren, J. Cebon, A. Dobrovic, J. M. Mariadason, A. Strasser, L. Rohrbeck, N. K. Haass, M. J. Herold and W. D. Fairlie, *Cell Death Dis*, 2019, **10**, 342.
21. S. Hedir, M. De Giorgi, J. Fogha, M. De Pascale, L. B. Weiswald, E. Brotin, B. Marekha, C. Denoyelle, C. Denis, P. Suzanne, F. Gautier, P. Juin, L. Ligat, F. Lopez, L. Carlier, R. Legay, R.

Bureau, S. Rault, L. Poulain, J. S. Oliveira Santos and A. S. Voisin-Chiret, *Eur J Med Chem*, 2018, **159**, 357-380.
22. C. Gloaguen, A. S. Voisin-Chiret, J. Sopkova-de Oliveira Santos, J. Fogha, F. Gautier, M. De Giorgi, G. Burzicki, S. Perato, C. Petigny-Lechartier, K. Simonin-Le Jeune, E. Brotin, D. Goux, M. N'Diaye, B. Lambert, M. H. Louis, L. Ligat, F. Lopez, P. Juin, R. Bureau, S. Rault and L. Poulain, *J Med Chem*, 2015, **58**, 1644-1668.
23. C. Petigny-Lechartier, C. Duboc, A. Jebahi, M. H. Louis, E. Abeilard, C. Denoyelle, P. Gauduchon, L. Poulain and M. Villedieu, *Mol Cancer Ther*, 2017, **16**, 102-115.
24. C. E. Weeden, C. Ah-Cann, A. Z. Holik, J. Pasquet, J. M. Garnier, D. Merino, G. Lessene and M. L. Asselin-Labat, *Oncogene*, 2018, **37**, 4475-4488.
25. M. L. Bonnefond, B. Lambert, F. Giffard, E. Abeilard, E. Brotin, M. H. Louis, M. S. Gueye, P. Gauduchon, L. Poulain and M. N'Diaye, *Apoptosis*, 2015, **20**, 535-550.
26. M. L. Bonnefond, R. Florent, S. Lenoir, B. Lambert, E. Abeilard, F. Giffard, M. H. Louis, N. Elie, M. Briand, D. Vivien, L. Poulain, P. Gauduchon and M. N'Diaye, *Oncotarget*, 2018, **9**, 33896-33911.
27. R. Beroukhim, C. H. Mermel, D. Porter, G. Wei, S. Raychaudhuri, J. Donovan, J. Barretina, J. S. Boehm, J. Dobson, M. Urashima, K. T. Mc Henry, R. M. Pinchback, A. H. Ligon, Y. J. Cho, L. Haery, H. Greulich, M. Reich, W. Winckler, M. S. Lawrence, B. A. Weir, K. E. Tanaka, D. Y. Chiang, A. J. Bass, A. Loo, C. Hoffman, J. Prensner, T. Liefeld, Q. Gao, D. Yecies, S. Signoretti, E. Maher, F. J. Kaye, H. Sasaki, J. E. Tepper, J. A. Fletcher, J. Tabernero, J. Baselga, M. S. Tsao, F. Demichelis, M. A. Rubin, P. A. Janne, M. J. Daly, C. Nucera, R. L. Levine, B. L. Ebert, S. Gabriel, A. K. Rustgi, C. R. Antonescu, M. Ladanyi, A. Letai, L. A. Garraway, M. Loda, D. G. Beer, L. D. True, A. Okamoto, S. L. Pomeroy, S. Singer, T. R. Golub, E. S. Lander, G. Getz, W. R. Sellers and M. Meyerson, *Nature*, 2010, **463**, 899-905.
28. D. Merino, J. R. Whittle, F. Vaillant, A. Serrano, J. N. Gong, G. Giner, A. L. Maragno, M. Chanrion, E. Schneider, B. Pal, X. Li, G. Dewson, J. Grasel, K. Liu, N. Lalaoui, D. Segal, M. J. Herold, D. C. S. Huang, G. K. Smyth, O. Geneste, G. Lessene, J. E. Visvader and G. J. Lindeman, *Sci Transl Med*, 2017 Aug 2;**9**(401):eaam7049.
29. A. Kotschy, Z. Szlavik, J. Murray, J. Davidson, A. L. Maragno, G. Le Toumelin-Braizat, M. Chanrion, G. L. Kelly, J. N. Gong, D. M. Moujalled, A. Bruno, M. Csekei, A. Paczal, Z. B. Szabo, S. Sipos, G. Radics, A. Proszenyak, B. Balint, L. Ondi, G. Blasko, A. Robertson, A. Surgenor, P. Dokurno, I. Chen, N. Matassova, J. Smith, C. Pedder, C. Graham, A. Studeny, G. Lysiak-Auvity, A. M. Girard, F. Grave, D. Segal, C. D. Riffkin, G. Pomilio, L. C. Galbraith, B. J. Aubrey, M. S. Brennan, M. J. Herold, C. Chang, G. Guasconi, N. Cauquil, F. Melchiore, N. Guigal-Stephan, B. Lockhart, F. Colland, J. A. Hickman, A. W. Roberts, D. C. Huang, A. H. Wei, A. Strasser, G. Lessene and O. Geneste, *Nature*, 2016, **538**, 477-482.
30. S. Caenepeel, S. P. Brown, B. Belmontes, G. Moody, K. S. Keegan, D. Chui, D. A. Whittington, X. Huang, L. Poppe, A. C. Cheng, M. Cardozo, J. Houze, Y. Li, B. Lucas, N. A. Paras, X. Wang, J. P. Taygerly, M. Vimolratana, M. Zancanella, L. Zhu, E. Cajulis, T. Osgood, J. Sun, L. Damon, R. K. Egan, P. Greninger, J. D. McClanaghan, J. Gong, D. Moujalled, G. Pomilio, P. Beltran, C. H. Benes, A. W. Roberts, D. C. Huang, A. Wei, J. Canon, A. Coxon and P. E. Hughes, *Cancer Discov*, 2018, **8**, 1582-1597.
31. A. E. Tron, M. A. Belmonte, A. Adam, B. M. Aquila, L. H. Boise, E. Chiarparin, J. Cidado, K. J. Embrey, E. Gangl, F. D. Gibbons, G. P. Gregory, D. Hargreaves, J. A. Hendricks, J. W. Johannes, R. W. Johnstone, S. L. Kazmirski, J. G. Kettle, M. L. Lamb, S. M. Matulis, A. K. Nooka, M. J. Packer, B. Peng, P. B. Rawlins, D. W. Robbins, A. G. Schuller, N. Su, W. Yang, Q. Ye, X. Zheng, J. P. Secrist, E. A. Clark, D. M. Wilson, S. E. Fawell and A. W. Hird, *Nat Commun*, 2018, **9**, 5341.
32. M. L. Stewart, E. Fire, A. E. Keating and L. D. Walensky, *Nat Chem Biol*, 2010, **6**, 595-601.
33. (a) N. A. Cohen, M. L. Stewart, E. Gavathiotis, J. L. Tepper, S. R. Bruekner, B. Koss, J. T. Opferman and L. D. Walensky, *Chem Biol*, 2012, **19**, 1175-1186; (b) L. D. Walensky, Patent WO2013/142281, 2013.
34. S. Varadarajan, M. Vogler, M. Butterworth, D. Dinsdale, L. D. Walensky and G. M. Cohen, *Cell Death Differ*, 2013, **20**, 1475-1484.
35. J. A. Kritzer, *Chem Biol*, 2012, **19**, 1082-1083.
36. J. L. Yap, L. Chen, M. E. Lanning and S. Fletcher, *J Med Chem*, 2017, **60**, 821-838.

37. D. D. Vo, F. Gautier, P. Juin and R. Grée, *Eur J Med Chem*, 2012, **51**, 286-293.
38. D. D. Vo, F. Gautier, S. Barillé-Nion, P. Juin, N. Levoin and R. Grée, *Tetrahedron*, 2014, **70**, 301–311.
39. D. D. Vo, F. Gautier, S. Barille-Nion, P. Juin, N. Levoin and R. Grée, *Bioorg Med Chem Lett*, 2014, **24**, 1758-1761.
40. N. Levoin, D. D. Vo, F. Gautier, S. Barille-Nion, P. Juin, O. Tasseau and R. Grée, *Bioorg Med Chem*, 2015, **23**, 1747-1757.
41. D. Duy Vo, I. Rouaud, F. Le Devehat, F. Gautier, S. Barille-Nion, P. Juin, N. Levoin, J. Boustie and R. Grée, *Med Chem*, 2016, **12**, 419-425.
42. P. K. Bose and B. K. Nandi, *J. Ind. Chem. Soc*, 1931, 3.
43. J. McLean and F. J. Wilson, *J Chem Soc*, 1937, 556-559. DOI: 10.1039/JR9370000556,
44. E. Bulka, H.-G. Rohde and H. Beyer, *Chem Ber*, 1965, **98**, 259-273.
45. S. Murru, C. B. Singh, V. Kavala and B. K. Patel, *Tetrahedron*, 2008, **64**, 1931-1942.
46. S. M. Abou-Seri, N. A. Farag and G. S. Hassan, *Chem Pharm Bull (Tokyo)*, 2011, **59**, 1124-1132.
47. M. M. Heravi and S. Moghimi, *Tetrahedron Lett*, 2012, **53**, 392-394.
48. T. W. Sanchez, B. Debnath, F. Christ, H. Otake, Z. Debyser and N. Neamati, *Bioorg Med Chem*, 2013, **21**, 957-963.
49. K. M. Khan, S. Qurban, U. Salar, M. Taha, S. Hussain, S. Perveen, A. Hameed, N. H. Ismail, M. Riaz and A. Wadood, *Bioorg Chem*, 2016, **68**, 245-258.
50. U. Salar, M. Taha, K. M. Khan, N. H. Ismail, S. Imran, S. Perveen, S. Gul and A. Wadood, *Eur J Med Chem*, 2016, **122**, 196-204.
51. S. Mirza, S. Asma Naqvi, K. Mohammed Khan, U. Salar and M. I. Choudhary, *Bioorg Chem*, 2017, **70**, 133-143.
52. C. Bodhak and A. Pramanik, *J Org Chem*, 2019, **84**, 7265-7278.
53. A. A. Hassan, N. K. Mohamed, A. A. Aly, H. N. Tawfeek, S. Bräse and M. Nieger, *J Mol Struct*, 2019, **1176**, 346-356.
54. N. Karali, A. Kocabalkanli, A. Gürsoy and O. Ateş, *Farmaco*, 2002, **57**, 589-593.
55. M. C. Cardia, S. Distinto, E. Maccioni, A. Plumitallo, M. L. Sanna, M. Saddi and A. Delogu, *J Heterocycl Chem*, 2006, **43**, 1337-1342.
56. S. Y. Abbas, A. A. Farag, Y. A. Ammar, A. A. Atrees, A. F. Mohamed and A. A. El-Henawy, *Monatsh Chem*, 2013, **144**, 1725-1733.
57. W.-D. Pfeiffer, K.-D. Ahlers, A. S. Saghyan, A. Villinger and P. Langer, *Helv Chim Acta*, 2014, **97**, 76-87.
58. W.-D. Pfeiffer, D. Junghans, A. S. Saghyan and P. Langer, *J Heterocyclic Chem*, 2014, **51**, 1063-1067.
59. S. N. Eman, M. E.-h. Salwa and R. Z. Eman, *Int J Pharm Pharm Sci*, 2015, **7**.
60. R. Meleddu, S. Distinto, A. Corona, E. Tramontano, G. Bianco, C. Melis, F. Cottiglia and E. Maccioni, *J Enzym Inhib Med Chem*, 2017, **32**, 130-136.
61. T. I. de Santana, M. O. Barbosa, P. Gomes, A. C. N. da Cruz, T. G. da Silva and A. C. L. Leite, *Eur J Med Chem*, 2018, **144**, 874-886.
62. M. A. Hussein, A. H. Kafafy, S. G. Abdel-Moty and O. M. Abou-Ghadir, *Acta Pharm*, 2009, **59**, 365-382.
63. J. B. Baell and G. A. Holloway, *J Med Chem*, 2010, **53**, 2719-2740.
64. C. Aldrich, C. Bertozzi, G. I. Georg, L. Kiessling, C. Lindsley, D. Liotta, K. M. Merz, Jr., A. Schepartz and S. Wang, *J Med Chem*, 2017, **60**, 2165-2168.
65. R. Wong and S. J. Dolman, *J Org Chem*, 2007, **72**, 3969-3971.
66. U. Mandapati, S. Pinapati and R. Rudraraju, *Tetrahedron Lett*, 2017, **58**, 4-128.
67. Ł. Janczewski, A. Gajda and T. Gajda, *Eur J Org Chem*, 2019, 2528-2532.
68. Z. Nikolovska-Coleska, R. Wang, X. Fang, H. Pan, Y. Tomita, P. Li, P. P. Roller, K. Krajewski, N. G. Saito, J. A. Stuckey and S. Wang, *Anal Biochem*, 2004, **332**, 261-273.
69. D. L. Mobley and J. P. Guthrie, *J Comput Aided Mol Des*, 2014, **28**, 711-720.
70. M. Karki and J. Magolan, *J Org Chem*, 2015, **80**, 3701-3707.
71. R. El Majzoub, M. Fayyad-Kazan, A. Nasr El Dine, R. Makki, E. Hamade, R. Gree, A. Hachem, R. Talhouk, H. Fayyad-Kazan and B. Badran, *Genes & Genomics*, 2019, **41**, 1431-1443.
72. M. A. G. B. Gomes, L. P. Carvalho, B. S. Rocha, R. R. Oliveira, E. J. T. de Melo and E. J. Maria, *Med Chem Res*, 2013, **22**, 3574-3580.
73. E. Fire, S. V. Gulla, R. A. Grant and A. E. Keating, *Protein Sci*, 2010, **19**, 507-519.
74. H. Zhou, J. Chen, J. L. Meagher, C. Y. Yang, A. Aguilar, L. Liu, L. Bai, X. Cong, Q. Cai, X. Fang, J.

A. Stuckey and S. Wang, *J Med Chem*, 2012, **55**, 4664-4682.
75. A. Miranker and M. Karplus, *Proteins*, 1991, **11**, 29-34.
76. M. K. Haider, H. O. Bertrand and R. E. Hubbard, *J Chem Inf Model*, 2011, **51**, 1092-1105.
77. A. Friberg, D. Vigil, B. Zhao, R. N. Daniels, J. P. Burke, P. M. Garcia-Barrantes, D. Camper, B. A. Chauder, T. Lee, E. T. Olejniczak and S. W. Fesik, *J Med Chem*, 2013, **56**, 15-30.
78. S. Desrat, C. Remeur and F. Roussi, *Org Biomol Chem*, 2015, **13**, 5520-5531.
79 L. Poulain, H. Lincet, F. Duigou, E. Deslandes, F. Sichel, P. Gauduchon and C. Staedel, *Int J Cancer*, 1998, **78**, 454-463.